Article

Mitochondrial RNA stimulates beige adipocyte development in young mice

Anh Cuong Hoang[1], László Sasi-Szabó[2], Tibor Pál [2], Tamás Szabó[2], Victoria Diedrich[1], Annika Herwig[1], Kathrin Landgraf [3], Antje Körner [3,4] & Tamás Röszer [1,2]✉

Childhood obesity is a serious public health crisis and a critical factor that determines future obesity prevalence. Signals affecting adipocyte development in early postnatal life have a strong potential to trigger childhood obesity; however, these signals are still poorly understood. We show here that mitochondrial (mt)RNA efflux stimulates transcription of nuclear-encoded genes for mitobiogenesis and thermogenesis in adipocytes of young mice and human infants. While cytosolic mtRNA is a potential trigger of the interferon (IFN) response, young adipocytes lack such a response to cytosolic mtRNA due to the suppression of IFN regulatory factor (IRF)7 expression by vitamin D receptor signalling. Adult and obese adipocytes, however, strongly express IRF7 and mount an IFN response to cytosolic mtRNA. In turn, suppressing IRF7 expression in adult adipocytes restores mtRNA-induced mitobiogenesis and thermogenesis and eventually mitigates obesity. Retrograde mitochondrion-to-nucleus signalling by mtRNA is thus a mechanism to evoke thermogenic potential during early adipocyte development and to protect against obesity.

Childhood obesity is a serious public health crisis today and is associated with an increased risk of adult obesity and diabetes, which is projected to affect ~58% of the world's adult population by 2030 (refs. [1–4]). Storing fat in adipocytes is necessary for metabolic and endocrine health; however, excess fat accumulation accounts for the development of metabolic diseases[1,2,4–6]. Infancy and early childhood (before 5.5 years of age) are critical periods that determine adipocyte number and fat accumulation, thereby also determining future obesity[7–9]. For example, an accelerated rate of body weight gain and overweight during the first year of life and in early childhood increase the probability of obesity and obesity-associated diseases in adulthood[1,2,5,6]. Signals that control adipocyte development in early postnatal life thereby have a strong potential to trigger obesity; however, these signals are still poorly understood.

The human foetus accumulates fat in subcutaneous adipose tissue depots at the last trimester, and fat becomes a relevant energy source at birth and in early postnatal life[10–12]. The foetus has a carbohydrate-based metabolism, which shifts to lipid-rich nutrition in the form of breast-feeding or formula feeding at birth[10–12]. The subcutaneous adipose tissue of a newborn is actively engaged in lipolysis and beta oxidation of fatty acids to generate energy[10–12]. Mammals are homoeothermic animals; hence the foetus develops in a thermally stable environment in the womb, without the demand of investing energy into the maintenance of its own core body temperature. However, this scenario rapidly changes at birth, when the newborn is challenged with a hypothermic environment without the ability to perform shivering thermogenesis. The large energy demand of homoeothermy is covered by burning off fat as heat in the adipose tissue, in a process often called non-shivering thermogenesis or adaptive thermogenesis[13]. It is estimated that the heat produced in a human term infant is generated mostly by fat (64%) catabolism in non-shivering thermogenesis[14,15]. The responsible thermogenic adipocytes produce heat from uncoupled oxidative

[1]Institute of Neurobiology, Ulm University, Ulm, Germany. [2]Institute of Pediatrics, Clinical Centre, Faculty of Medicine, University of Debrecen, Debrecen, Hungary. [3]Center for Pediatric Research, University Hospital for Children and Adolescents, University of Leipzig, Leipzig, Germany. [4]Helmholtz Institute for Metabolic, Obesity and Vascular Research (HI-MAG) of the Helmholtz Center München at the University of Leipzig and University Hospital Leipzig, Leipzig, Germany. ✉e-mail: tamas.roeszer@uni-ulm.de

phosphorylation in their extensive mitochondrial network, using lipids as metabolic fuel[12,16]. Thermogenic adipocytes are distributed in the subcutaneous fat depots of a newborn[17] and are still detectable in early childhood[12,16]. By contrast, adult humans have shivering thermogenesis, and subcutaneous adipose tissue depots function as thermal insulators and long-term storage sites of fat[17]. Adipocytes of subcutaneous fat depots in adults are therefore poor in mitochondria and accumulate lipids instead of metabolizing them to energy or heat[18].

Thermogenic adipocytes in human subcutaneous adipose tissue progressively disappear by the age of 5–7 years, when adipose tissue expansion occurs as a physiological process[1,2,7]. Subcutaneous fat depots of young mice are rich in thermogenic adipocytes, which disappear by weaning age[16]. This trait of young mice resembles the development of thermogenic fat cells in humans, making them suitable models to study mechanisms of early-life human adipocyte development. Recent studies suggest that premature loss of thermogenic fat cells is associated with early onset of adipose tissue expansion, and these two factors together may lead to childhood obesity[1,2,7,12,16]. It is plausible that delaying or reverting the metabolic shift from fat catabolism and thermogenesis to fat storage has therapeutic potential in obesity prevention[1,2,12,16].

The conversion of fat into energy and heat requires an extensive mitochondrial network[19,20], and, accordingly, adipocytes of the subcutaneous adipose tissue are rich in mitochondria in early postnatal life[10,15]. However, the abundance of mitochondria is associated with a potentially inflammation-provoking efflux of mtDNA to the cytosol[21]. Due to its endosymbiotic origin, mtDNA resembles prokaryote-type DNA and eventually triggers an IFN response[22–25]. Obese adipocytes produce IFNs, and IFNs eventually trigger metabolic diseases[26,27]. IFNs may damage the mitochondrial network and the capacity for fat oxidation and thermogenesis and trigger metabolic inflammation and insulin resistance[28,29]. It has been shown that activation of the stimulator of IFN-response genes (STING) pathway (a major cytosolic DNA-sensing pathway) worsens obesity and abrogates the thermogenic programme in adipocytes[30]. In turn, inhibition of mtDNA efflux into the adipocyte cytosol effectively reduces obesity-associated inflammation and insulin resistance[31].

The efflux of mtDNA is inevitably associated with the release of mtRNA, which contains double-stranded RNA (dsRNA) motifs, strong inducers of the IFN response[22–25]. Given the abundance of mitochondria in adipocytes of young mice and human infants[32], we asked whether these cells have a unique signalling mechanism that supports their mitochondrial network by mitigating the IFN response to mtRNA. While exploring this, we unexpectedly found that cytosolic mtRNA activated mitochondrion-to-nucleus signalling in adipocytes, which stimulated expression of nuclear-encoded genes of mitobiogenesis and thermogenesis in young mice and human infants. The IFN response to mtRNA was lacking in young adipocytes, plausibly due to the suppression of IRF7 by vitamin D receptor (VDR) signalling. Adult and obese adipocytes, however, expressed IRF7 strongly, and they mounted an IFN response to cytosolic mtRNA, abrogating its signalling role to stimulate mitobiogenesis and thermogenesis. In turn, when we inhibited IRF7 expression with VDR activation and transfected adipocytes with mtRNA, we could effectively induce beige adipogenesis and mitigate obesity in mice. Retrograde mitochondrion-to-nucleus signalling by mtRNA is hence a new mechanism that controls early adipocyte development and protects against obesity.

Results

Young adipocytes are immune tolerant for cytosolic mtRNA

We found that inguinal adipocytes of young mice at postnatal day 6 contained more mitochondria and higher levels of cytosolic mtRNA than their adult counterparts (Fig. 1a and Extended Data Fig. 1a), suggesting that the cytosolic mtRNA level was proportional to the amount of mitochondria. Cytosolic mtRNA, due to the abundance of its dsRNA motifs

(Extended Data Fig. 1a), triggers an IFN response[21,23–25,33,34] (Fig. 1b). However, transfecting young (postnatal day 6) adipocytes with mtRNA failed to induce such a response (Fig. 1c and Extended Data Fig. 1a). In turn, adipocytes of adult mice (8 weeks of age) mounted a robust IFN response to cytosolic mtRNA (Fig. 1c and Extended Data Fig. 1a).

There are controversial findings about the effect of IFNs on mitochondrial energy and heat production[35–38]. To test the effect of IFN-β on adipocyte mitochondria, we cultured subcutaneous adipocytes of adult mice and non-obese, non-diabetic humans (age range, 16–17 years) and subjected them to IFN-β treatment. We used IFN-β at a concentration corresponding to the level of IFN-β secreted by adult mouse adipocytes in response to mtRNA transfection (Extended Data Fig. 1a). We found that IFN-β triggered mitochondrial damage and adipocytes exhibited signs of mitophagy (Fig. 1d and Extended Data Fig. 1b). IFN-β compromised mitochondrial mass (Fig. 1e) and reduced the level of the mitochondrial enzymes cyclooxygenase I (COX-I) and succinate dehydrogenase A (SDH-A) in both mouse and human adipocytes (Fig. 1f). Moreover, IFN-β treatment supported fat accumulation in preadipocytes (Fig. 1g). Coherently, hypertrophic human adipocytes had robust IFN-β expression (Fig. 1h). These effects of IFN-β on mitochondria[37] and the robust expression of IFN-β by hypertrophic adipocytes agree with the findings that obesity development is associated with prominent expression of IFNs and IFN-stimulated genes (ISGs) in adipocytes[29,31].

It is known that cytosolic mtRNA triggers *Ifnb* (*Ifnb1*) expression through cytosolic RNA sensors such as retinoic acid-inducible gene I (RIG-I) and RIG-I-like melanoma differentiation-associated protein 5 (MDA5)[24]. Accordingly, transfecting adult adipocytes with a synthetic ligand of cytosolic RNA sensors, so-called poly(deoxyadenylic-deoxythymidylic) acid (poly(dA:dT))[39], increased *Ifnb* transcription to the same magnitude as cytosolic mtRNA (Fig. 1i). Cytosolic poly(dA:dT) is transcribed into RNA by the activity of RNA polymerase III, allowing stimulation of cytosolic RNA sensors[39] (Extended Data Fig. 1c). Furthermore, cytosolic poly(dA:dT) mimicked the effect of IFN-β on adipocyte mitochondria in mice and humans (Fig. 1j,k). Conversely, an IFN-β-blocking antibody protected both mouse and human adipocytes from poly(dA:dT)-induced mitochondrial damage and slightly increased the levels of COX-I and SDH-A (Fig. 1j,k).

Importantly, neither cytosolic mtRNA (Fig. 1c) nor cytosolic poly(dA:dT) induced *Ifnb* transcription in young mouse adipocytes (Fig. 1l). Coherently, young mouse adipocytes were protected from mitochondrial damage induced by cytosolic poly(dA:dT) (Fig. 1m). This difference could not be explained by the absence of MDA5 or RIG-I in young adipocytes or by the inability of young adipocytes to be transfected with poly(dA:dT) (Extended Data Fig. 1c–f).

When we transfected adipocytes from human infants (aged 0–1 year), children (2–11 years) and adolescents (15–17 years) with poly(dA:dT), we found that adipocytes of infants and children were resistant to mitochondrial damage (Fig. 1n), similar to the adipocytes of young mice. Indeed, adipocytes of infants, similar to adipocytes of young mice, increased their COX-I and SDH-A levels following poly(dA:dT) transfection (Fig. 1m,n). In adipocytes of adolescents, however, cytosolic poly(dA:dT) reduced COX-I and SDH-A levels (Fig. 1n), mirroring poly(dA:dT) effects on adult mouse adipocytes (Fig. 1m).

Young adipocytes have suppressed IRF7 expression

Transcription of *Ifnb* is initiated by IRF3 and IRF7, which trigger the IFN response by forming homodimers or heterodimers[40,41]. Accordingly, the absence of adipocyte *Irf3* or *Irf7* was equally protective from mitochondrial damage in response to cytosolic poly(dA:dT) (Fig. 2a).

We next measured transcription of *Irf3* and *Irf7* in adipocytes of young and adult mice. The transcript levels of *Irf3* were similar in young and adult adipocytes; however, the level of *Irf7* was magnitudes higher in adult adipocytes than in their young counterparts (Fig. 2b and Extended Data Fig. 2a). In adult adipocytes, IRF7 appeared in the
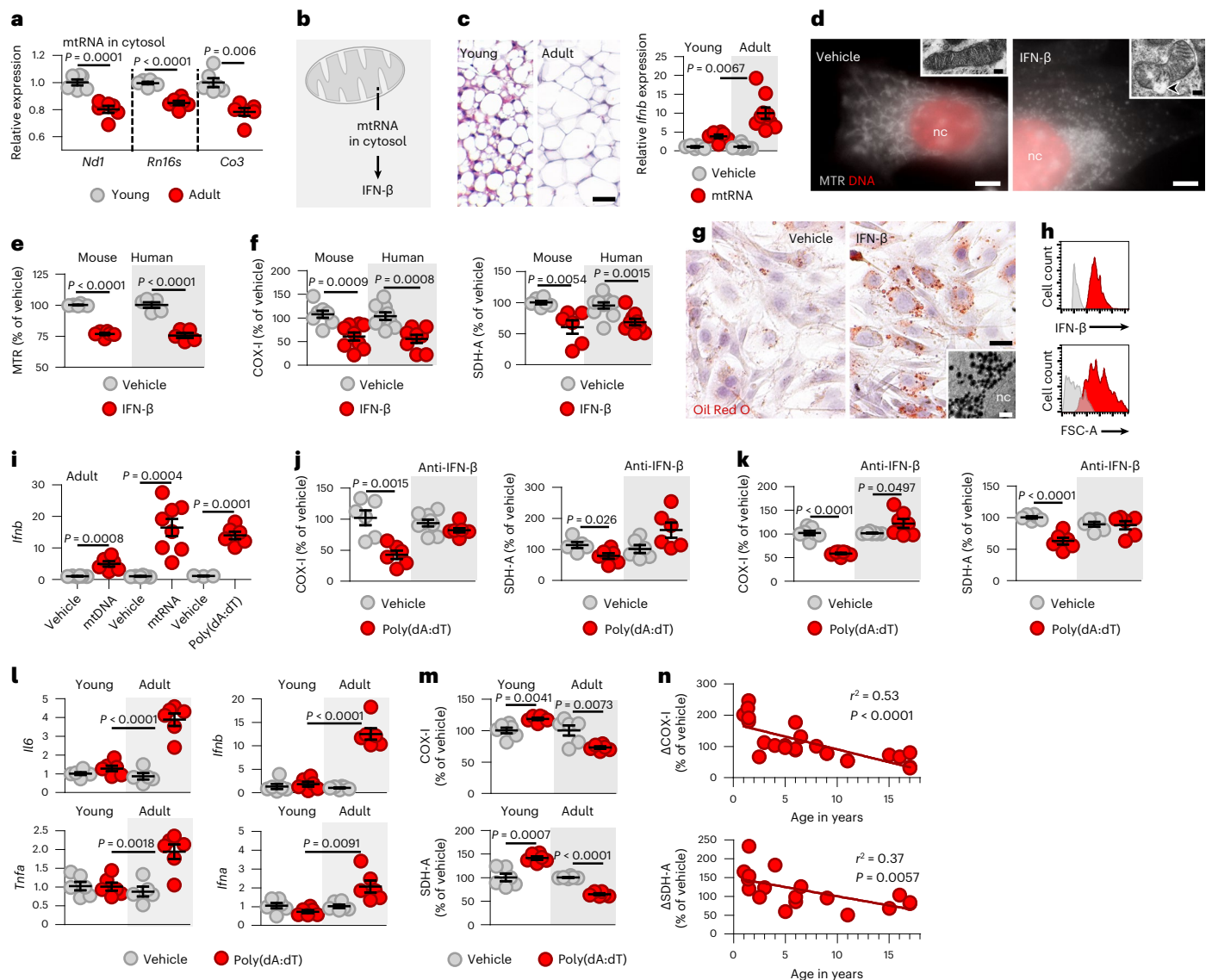
Fig. 1 | mtRNA does not trigger inflammation in young adipocytes. a, mtRNA in the cytosol of inguinal adipocytes of young (postnatal day 6) and adult (postnatal day 56) mice. *Rn16s* is also known as *Mt-Rnr2*. **b**, Cytosolic mtRNA potentially triggers an IFN response that is mediated by cytosolic RNA-sensor proteins, such as RIG-I and MDA5. **c**, Histology of young and adult mouse inguinal adipose tissue, hematoxylin and eosin (H&E); scale bar, 25 µm. Young and adult adipocytes of the same fat depot were transfected with mtRNA (2 µg ml⁻¹, 18 h) and the transcript levels of *Ifnb* were measured. **d**, Effect of IFN-β on the mitochondrial network in adult mouse adipocytes. Cells were treated with vehicle or 125 IU ml⁻¹ IFN-β for 18 h, and mitochondria were labelled with MitoTracker Red (MTR). Scale bar, 20 µm. Inserts show transmission electron microscopy images of mitochondria; scale bar, 20 nm. Arrow head indicates mitochondrial swelling. **e**, Effect of IFN-β on mitochondrial mass in adult mouse and human adipocytes, measured by MTR staining intensity. **f**, Effect of IFN-β on the level of mitochondrial encoded COX-I and nuclear-encoded SDH-A in adult mouse and human adipocytes. **g**, Effect of IFN-β on fat accumulation in mouse preadipocytes. Oil Red O labelling of lipid droplets. Scale bar, 50 µm. Insert shows electron microscopy of the lipid-rich cytoplasm. nc, nucleus. Scale bar, 20 nm. **h**, Flow cytometry histogram of human

adipocyte IFN-β content and forward scatter area (FSC-A, proportional to cell size). **i**, Transcription of *Ifnb* in adult mouse adipocytes in response to 18-h-long transfection with 5 µg ml⁻¹ mtDNA, mtRNA or poly(dA:dT). **j**, Levels of COX-I and SDH-A in adult mouse adipocytes following transfection with poly(dA:dT). Anti-IFN-β, presence of neutralizing antibody against IFN-β. **k**, Levels of COX-I and SDH-A in adult human adipocytes following transfection with poly(dA:dT). Anti-IFN-β, presence of neutralizing antibody against IFN-β. **l**, Transcription of IFN-response genes in young and adult mouse adipocytes in response to transfection with poly(dA:dT). *Ifna* is also known as *Ifna1*; *Tnfa* is also known as *Tnf*. **m**, Levels of COX-I and SDH-A in young and adult mouse adipocytes following transfection with poly(dA:dT). **n**, Correlation of donor age and the corresponding changes in COX-I and SDH-A levels in human adipocytes following transfection with poly(dA:dT). Data represented as mean ± s.e.m. *n* = 6 (**a**), *n* = 6 young and *n* = 9 adult samples (**b**), *n* = 6 mouse and *n* = 5 human samples (**e**), *n* = 9 (**f**), *n* = 7 and 8 (for mtRNA) (**i**), *n* = 6 (**j**–**m**), *n* = 25 (for COX-I) and *n* = 24 (for SDH-A) biologically independent experiments (**n**). Assays shown in **d**,**g**,**h** were repeated four times. Statistical significance was determined using Student's two-tailed unpaired *t*-test (**a**,**c**,**e**,**f**,**i**–**m**) or linear regression analysis (**n**).

cytoplasm and in the nucleus, and, upon stimulation, IRF7 translocated to the nucleus and become phosphorylated (Extended Data Fig. 2b–e). In children, the adipose tissue level of *IRF7* mRNA was strongly increased by overweight and obesity (body mass index standard deviation score over 1.28), while the level of *IRF3* mRNA was

unrelated to obesity status (Fig. 2c). Accordingly, hypertrophic human adipocytes strongly expressed IRF7 protein (Fig. 2d), along with IFN-β (Fig. 1h). This is in agreement with previous findings suggesting that IRF3 is expressed constitutively, whereas IRF7 is an ISG[42]. The association of IRF7 expression with IFN-β⁺ hypertrophic adipocytes further
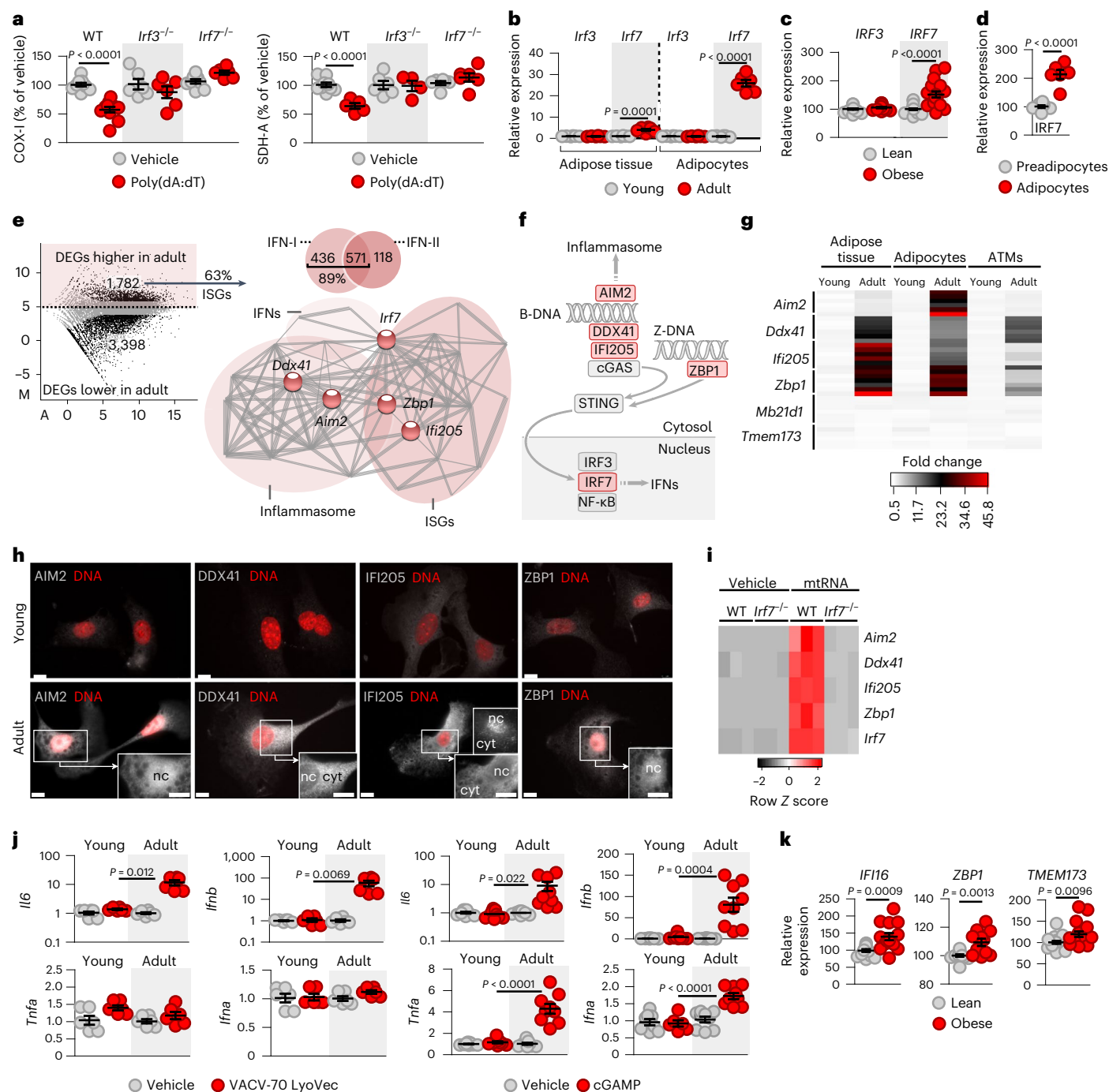
Fig. 2 | IRF7 is key for the IFN response to cytosolic mtRNA in adipocytes.
a, Levels of COX-I and SDH-A in adipocytes following transfection with poly(dA:dT). *Irf3*$^{-/-}$, adipocytes deficient in IRF3; *Irf7*$^{-/-}$, adipocytes deficient in IRF7. **b**, Relative expression levels of *Irf3* and *Irf7* mRNA in inguinal adipose tissue and in adipocytes of young and adult mice. **c**, Expression levels of *IRF3* and *IRF7* mRNA in the adipose tissue of children, 0.3–6.9 years of age. **d**, IRF7 protein levels in human preadipocytes and hypertrophic adipocytes, shown in Fig. 1h. **e**, Volcano plot of differentially expressed genes (DEGs) of young and adult mouse subcutaneous adipose tissue. IFN-I, type I ISGs; IFN-II, type II ISGs. Protein–protein interaction network of differentially expressed genes over-represented in adult adipose tissue. IRF7 had a central position by interconnecting gene networks of IFNs, ISGs and inflammasome components. **f**, Signal pathways of IRF7-target genes. Gene products over-represented in adult mice are indicated in red. **g**, Transcription of IRF7-target genes in young

adult mouse adipose tissue, adipocytes and adipose tissue macrophages (ATMs). *Mb21d1* is also known as *Cgas*, *Tmem173* as *Sting1*. **h**, Protein expression of IRF7-target genes in young and adult mouse adipocytes. cyt, cytosol; nc, nucleus; scale bar, 10 μm. **i**, Transcription of IRF7-target genes in mouse adipocytes transfected with mtRNA for 18 h. WT, wild-type; *Irf7*$^{-/-}$, adipocytes deficient in IRF7. **j**, Response of young and adult mouse adipocytes to cytosolic DNA. Adipocytes were transfected with 1 μg ml^{-1} VACV-70, a ligand of IFI205, for 18 h or with 10 μg ml^{-1} cGAMP, a ligand of STING, for 2 h. **k**, Transcription of IRF7-target genes in subcutaneous adipose tissue in children, 0.3–6.9 years of age. Data are represented as mean ± s.e.m. *n* = 6 (**a**,**b**,**d**,**g**,**j**, left), *n* = 15 (**c**), *n* = 9 (**j**, right), *n* = 15 lean and *n* = 14 obese (**k**), *n* = 3 (**i**) biologically independent samples. The assay shown in **h** was repeated six times. Statistical significance was determined using Student's two-tailed unpaired *t*-test and one-way ANOVA with Dunnett's post-hoc test.

supports this idea. Neutralizing IFN-β mitigated IRF7 protein expression in adipocytes in vitro (Extended Data Fig. 2f).

IRF7 plays a major role in the induction of the IFN response, even in the absence of IRF3. In turn, the IRF3-mediated IFN response remains minimal without the presence of even low amounts of IRF7 (ref. [42]), underscoring the fact that IRF7 deficiency of young adipocytes is plausibly responsible for the lack of IFN response to mtRNA. Nevertheless, the importance of IRF7 in the regulation of IFN-β expression may depend on the immune context and the cell type[41,43]; thus we continued to define a possible role of IRF7 in the IFN response of adipocytes.

When we surveyed the transcriptional landscape of young and adult mouse inguinal adipocytes using next-generation sequencing (NGS), we found that an extensive, IRF7-associated gene network was strongly over-represented in adult adipocytes (Fig. 2e and Extended Data Fig. 2g). This gene network contained ISGs, genes encoding inflammasome components and IFNs (Fig. 2e). The most over-represented genes of this IRF7-associated network were *Aim2*, *Ddx41*, *Zbp1* and *Ifi205*, all of which are essential for the IFN response (Fig. 2f).

In brief, *Aim2* encodes the IFN-inducible protein absent in melanoma 2 (AIM2), which triggers cytosolic DNA inflammasome assembly[44] (Fig. 2f). *Ddx41* encodes DEAD-box helicase 41 (DDX41), which recognizes cytosolic B-DNA and stimulates the IFN response (Fig. 2f). *Zbp1* encodes Z-DNA-binding protein 1 (ZBP1), also termed DAI[45], which recognizes cytosolic Z-DNA (Fig. 2f), a prevalent form of DNA in the cytosol of transcriptionally active cells[46]. *Ifi205* encodes IFN-γ-inducible protein 205 (IFI205), the murine equivalent of the human IFI16 protein[44], which recognizes cytosolic B-DNA and stimulates the IFN response (for details of the mouse strain-specific nomenclature of this protein, see Extended Data Fig. 2h)[40,41].

The increase in the expression of this IRF7-associated gene network was confined to adipocytes (Fig. 2g) and was lacking in other cell types and organs that we tested (Extended Data Fig. 2i–k). Consistently, the AIM2, DDX41, IFI205 and ZBP1 proteins were minimally expressed in young adipocytes (Fig. 2h). In turn, AIM2, DDX41, IFI205 and ZBP1 were present in the perinuclear region and in the cytoplasm of adult adipocytes, coherent with their known role in monitoring specific subcellular compartments (Fig. 2h)[45,47]. Induced transcription of *Aim2*, *Ddx41*, *Zbp1*, *Ifi205* and *Irf7* was dependent on IRF7 (Fig. 2i), and coherently, the promoter regions of these genes contained IRF7-binding sequences (Extended Data Fig. 2l). The levels of IRF7-associated ISG-encoding transcripts, including *IFI16*, *ZBP1* and *TMEM173* (*STING1*), were increased in the adipose tissue of children with obesity (Fig. 2k), reflecting their elevated *IRF7* levels (Fig. 2c).

It is intriguing that the main function of this IRF7-associated gene network is to initiate the IFN response to cytosolic DNA, rather than to cytosolic dsRNA[48]. Consistently, cytosolic DNA failed to trigger an IFN response in young adipocytes (Fig. 2j) and in adipocytes lacking IRF7 expression (Extended Data Fig. 2m). As mtRNA efflux is inevitably associated with the escape of mtDNA to the cytosol[21], this finding suggests that young adipocytes may be protected from an immune response to mtDNA, a known mechanism triggering obesity and obesity-induced metabolic diseases[31].

Altogether, these findings indicate that young adipocytes are protected from an immune response to cytosolic mtRNA. This immune tolerant state was concomitant with the suppression of IRF7-controlled genes of the IFN response.

Suppressed IRF7 signalling favours beige adipogenesis

To further elucidate the role of IRF7 in adipocyte development, we analysed the subcutaneous adipose tissue morphology of mice lacking IRF7. In the absence of IRF7, mice had abundant beige adipocytes with strong uncoupling protein 1 (UCP1) expression, resembling the morphology of brown adipose tissue (Fig. 3a). Coherently, brown adipose tissue in adult mice was naturally deficient in *Irf7* and did not respond to cytosolic poly(dA:dT) with *Ifnb* expression (Extended Data Fig. 3a,b),

in agreement with previous findings on a suppressed innate immune response in brown adipose tissue of mice[11,49,50].

Beige adipocytes are thermogenic; thus they help to dissipate energy stored in fat and eventually reduce body fat. The abundance of thermogenic adipocytes in IRF7-deficient mice is consistent with a previous finding that IRF7-deficient mice are protected from obesity[43]. IRF7-deficient adipocytes had increased expression of nuclear-encoded mitochondrial SDH-A (Fig. 3b), indicating increased mitobiogenesis. Moreover, adipocytes lacking IRF7 were protected from *Ifnb* expression triggered by cytosolic mtRNA (Fig. 3c). Of note, inguinal adipose tissue of young mice was rich in beige adipocytes, and adipocytes of young mice expressed signature genes of the thermogenic differentiation programme (Extended Data Fig. 4b–e). Adipocytes of lean children (1–4 years) were protected from IFN-β synthesis in response to cytosolic mtRNA and expressed UCP1, unlike adipocytes isolated from adolescents (16–17 years) (Fig. 3d,e and Extended Data Fig. 4f).

In summary, cytosolic mtRNA did not trigger IFN-β synthesis in young adipocytes. This trait was phenocopied by IRF7 deficiency and was associated with a thermogenic adipocyte phenotype. In mice, thermogenic fat cells were naturally deficient in IRF7, while, in humans, obesity increased the level of adipocyte IRF7.

Assuming that cytosolic mtRNA may play a role in the acquisition of the thermogenic phenotype, we next tested the effect of cytosolic mtRNA on the expression of genes required for mitochondrial thermogenesis and mitobiogenesis in young adipocytes. Cytosolic mtRNA triggered robust expression of *Ucp1* and genes associated with beige adipocytes (Fig. 3f): *Ppargc1a*, encoding the mitobiogenesis-stimulating peroxisome proliferator-activated receptor γ coactivator 1α; *Cidea*, encoding cell death-inducing DFFA-like effector A; and *Dio2*, encoding iodothyronine deiodinase 2. In young adipocytes, these responses occurred without induction of a robust immune response (Fig. 1c), and, ultimately, cytosolic mtRNA enhanced mitobiogenesis and the mitochondrial content of the adipocytes and stimulated mitochondrial thermogenesis (Fig. 3f,g). Similarly, cytosolic mtRNA increased mitobiogenesis, mitochondrial content and thermogenesis in adipocytes isolated from lean children (Fig. 3h), effects lacking in adipocytes of adolescents (Fig. 3i).

Cytosolic mtRNA may activate signalling through RIG-I and MDA5 (refs. [33,34]). Coherently, synthetic activators of RIG-I and MDA5 triggered transcription of beige genes in adipocytes (Fig. 3j and Extended Data Fig. 5a–c), whereas cytosolic mtRNA was ineffective in inducing beige gene expression in adipocytes lacking RIG-I or MDA5 (Fig. 3j). Cytosolic single-stranded RNA or stimulation of cell membrane-associated Toll-like receptor 3 (TLR3) failed to mimic the effects of cytosolic mtRNA on beige gene transcription (Extended Data Fig. 5d,e). These findings show that only double-stranded, cytosolic RNA molecules can induce mitobiogenesis, plausibly via retrograde signalling from mitochondria to the nucleus. Provided the abundance of double-stranded motifs in mtRNA molecules, this finding further confirms the signalling role of mtRNA in the cytosol. RIG-I and MDA5 activation by mtRNA or synthetic ligands triggered *Il6* expression (Extended Data Fig. 6a), which is a known autocrine–paracrine signal of thermogenic adipocyte development[16,51,52] (Extended Data Fig. 6b,c,e). Accordingly, blocking IL-6 signalling diminished the effect of mtRNA on beige adipogenesis (Extended Data Fig. 6d,f).

Notably, the absence of RIG-I or MDA5 compromised the expression of the nuclear-encoded mitochondrial SDH-A in adipocytes (Fig. 3j), suggesting that the mitochondrion-to-nucleus signalling role of mtRNA was lacking. Coherently, lack of RIG-I or MDA5 led to the loss of beige adipocytes in young mice (Fig. 3k).

Cytosolic mtRNA is, therefore, a strong inducer of beige features in young adipocytes by stimulating the expression of nuclear-encoded transcripts of mitobiogenesis and mitochondrial thermogenesis.
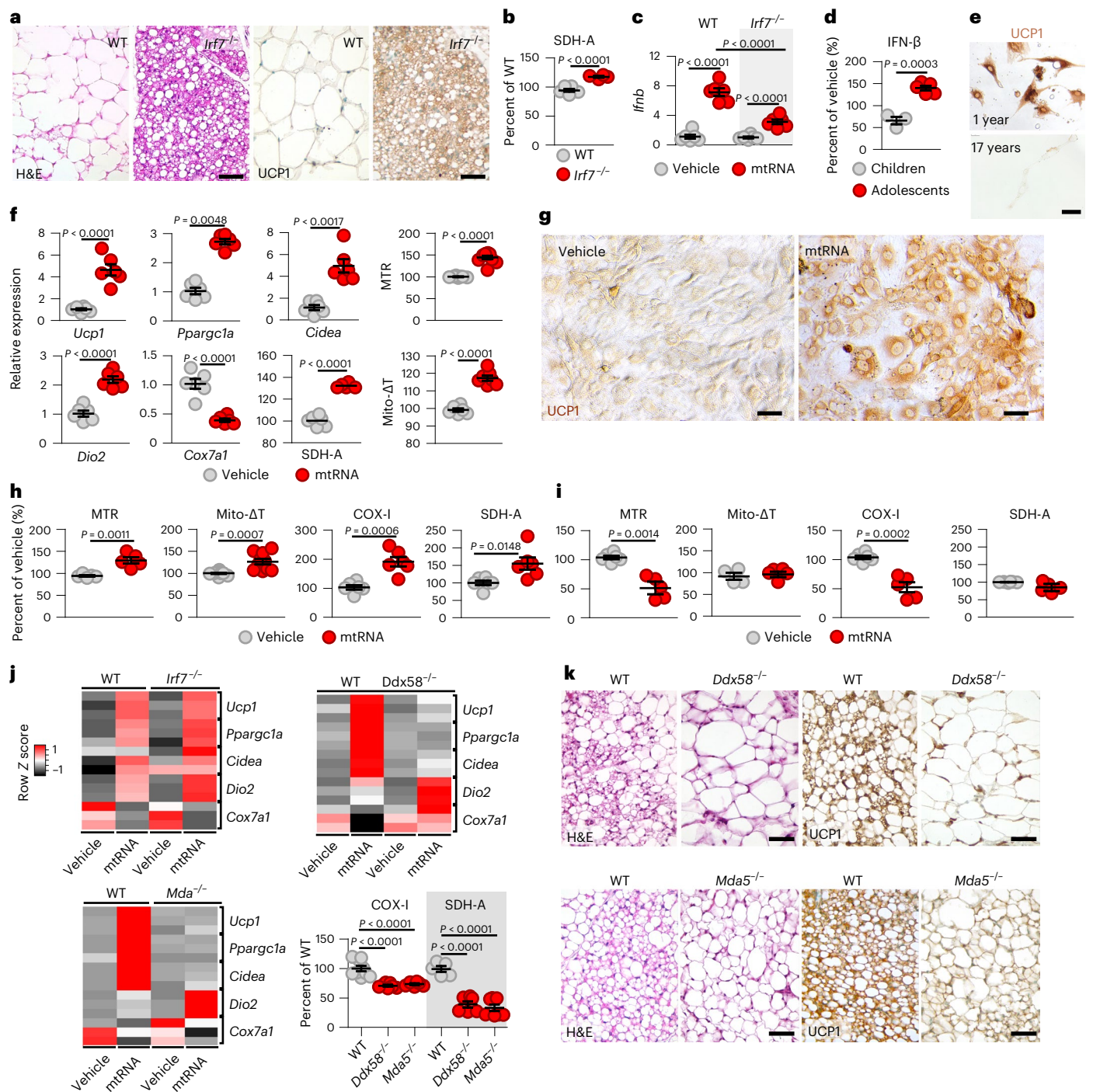
Fig. 3 | Cytosolic mtRNA induces beige adipocyte development. a, Histology of the inguinal adipose tissue of adult WT and IRF7-deficient *(Irf7⁻/⁻)* mice. UCP1, immunostaining of UCP1. Scale bar, 25 μm. **b,** Relative amount of the nuclear-encoded mitochondrial SDH-A in WT and *Irf7⁻/⁻* adipocytes. **c,** *Ifnb* transcription of WT and *Irf7⁻/⁻* adult adipocytes following transfection with vehicle or mtRNA (2 μg ml⁻¹, 4 h). **d,** IFN-β protein expression of adipocytes from children (1–9 years) and adolescents (16–17 years), transfected with mtRNA. **e,** UCP1 immunostaining of adipocytes isolated from a 1-year-old and a 17-year-old donor. Scale bar, 50 μm. **f,** Transcription of mitobiogenesis and thermogenesis genes in young mouse adipocytes following transfection with vehicle or mtRNA (2 μg ml⁻¹, 18 h). MTR, MTR fluorescence intensity, which is proportional to the amount of mitochondria. Mito-ΔT, mitochondrial temperature change, assessed with MitoThermoYellow staining. **g,** UCP1 immunostaining of mouse adipocytes transfected with vehicle or mtRNA for 18 h. Scale bar, 50 μm. **h,** Cytosolic delivery of 2 μg ml⁻¹ mtRNA into adipocytes of human infants (1–2.5 years of age) and its effect on mitobiogenesis. MTR, MTR fluorescence

intensity; Mito-ΔT, assessed with MitoThermoYellow staining; COX-I, COX-I activity; SDH-A, SDH-A activity. **i,** Cytosolic delivery of 2 μg ml⁻¹ mtRNA into adipocytes of human adolescents (16–17 years of age), and its effect on mitobiogenesis. **j,** Heatmap showing expression levels of beige adipocyte genes in WT, *Irf7⁻/⁻*, RIG-I-deficient *(Ddx58⁻/⁻)* and MDA5-deficient *(Mda5⁻/⁻)* adipocytes transfected with vehicle or 2 μg ml⁻¹ mtRNA for 18 h. Relative levels of mitochondrially encoded COX-I and nuclear-encoded SDH-A in young WT, *Ddx58⁻/⁻* and *Mda5⁻/⁻* adipocytes. Each data point represents adipocytes collected from five to seven mice. **k,** Histology of subcutaneous adipose tissue in young WT, *Ddx58⁻/⁻* and *Mda5⁻/⁻* mice. Note the absence of beige (multilocular) adipocytes in *Ddx58⁻/⁻* and *Mda5⁻/⁻* mice. Scale bar, 25 μm. Data are represented as mean ± s.e.m. *n* = 6 (**b,c,f,h** (COX-I and SDH-A levels), **j**), *n* = 5 (**d,h** (MTR and Mito-ΔT levels)) biologically independent samples. Assays shown in **a,e,g,k** were repeated six times. Heatmaps in **j** represent three replicates of independent analyses. Statistical significance was determined using Student's two-tailed unpaired *t*-test (**b–d,f,h**) or one-way ANOVA with Dunnett's post-hoc test (**j**).
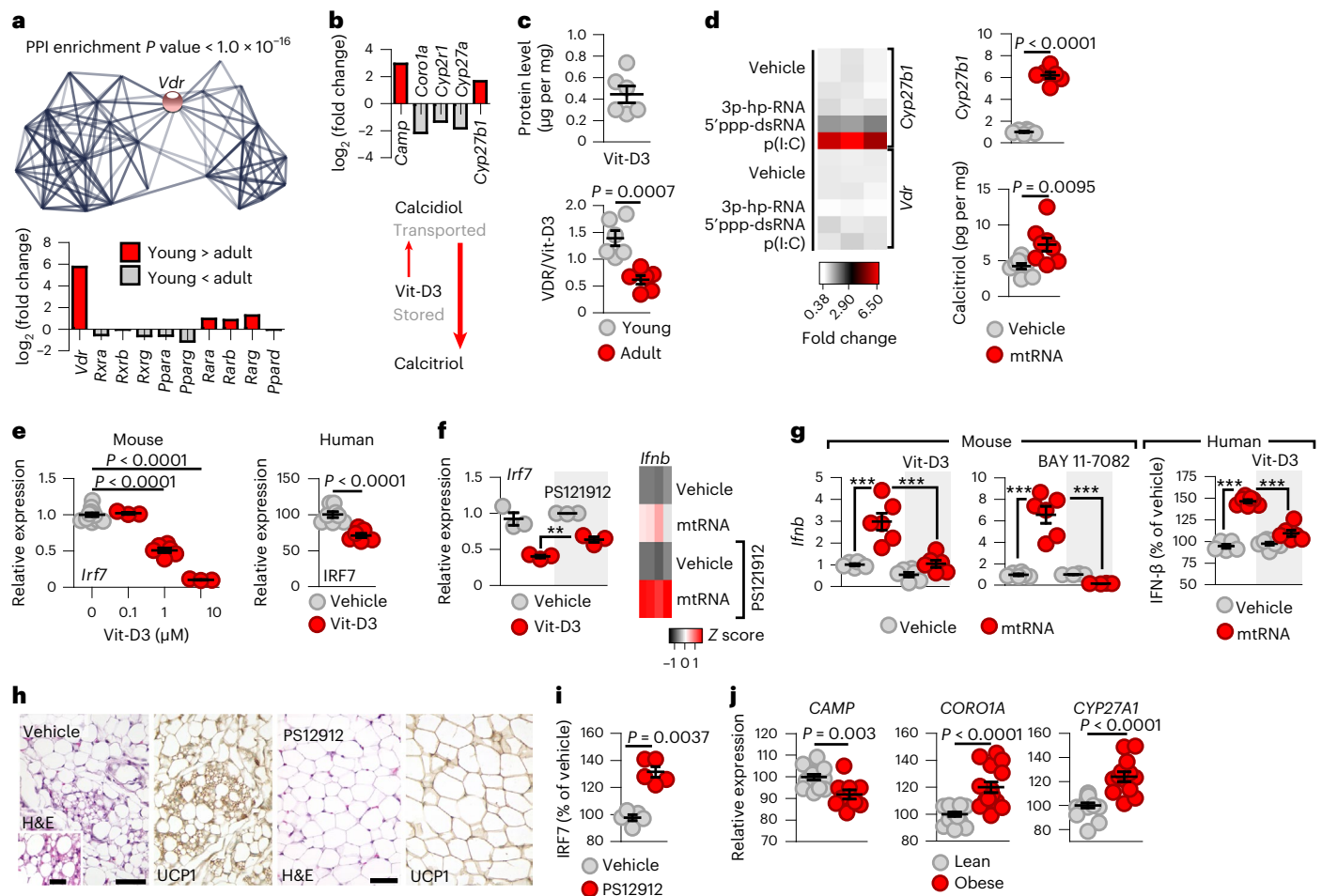
Fig. 4 | VDR diminishes IRF7 expression in young adipocytes. a, Genes over-represented in young mouse adipocytes belonged to the network associated with VDR signalling. Top, interactome map of gene products over-represented in young adipocytes. Bottom, comparison of young versus adult transcript levels of VDR and other nuclear receptors. PPI, protein–protein interaction network. **b**, Top, young versus adult transcript level of VDR-controlled genes and vitamin D metabolism genes. Bottom, scheme summarizing the dominant pathway of vitamin D metabolism in young mouse adipocytes. **c**, Level of Vit-D3 and the ratio of VDR/Vit-D3 in young mouse adipose tissue. **d**, Level of calcitriol-synthesizing *Cyp27b1* and *Vdr* in response to various cytosolic RNA species. 3p-hp-RNA, 5′ triphosphate hairpin RNA; 5′ppp-dsRNA, 5′ triphosphate double-stranded RNA; p(I:C), cytosolic polyinosinic:polycytidylic acid. Effect of cytosolic mtRNA on expression of *Cyp27b1* and Vit-D3–calcitriol converting activity (produced calcitriol per mg protein per min) of adipocytes transfected with vehicle or 2 µg ml⁻¹ mtRNA for 18 h. **e**, Effect of 2 µg ml⁻¹ cytosolic mtRNA on *Irf7*

transcription in mouse adipocytes and IRF7 levels in human adipocytes. **f**, Effect of Vit-D3 on *Irf7* and *Ifnb* transcription in mouse adipocytes. mtRNA, transfection with 2 µg ml⁻¹ mtRNA; PS121912, VDR inhibitor. **P = 0.0051. **g**, Response of mouse adipocytes pretreated with 1 µM Vit-D3 to cytosolic mtRNA. BAY 11-7082, NF-κB inhibitor. Response of human adipocytes treated with vehicle or Vit-D3 to cytosolic mtRNA. **h**, Histology of inguinal adipose tissue of young mice treated with vehicle or PS121912 for 5 d. Scale bar, 25 µm. **i**, Adipocyte IRF7 protein level of young mice treated with vehicle or PS121912 for 5 d. **j**, VDR-controlled gene expression in human subcutaneous adipose tissue, 0.3–6.9 years of age. Data are represented as mean ± s.e.m., and each data point represents a biological replicate. *n* = 6 (**c**); *n* = 3 in the heatmap, *n* = 6 for *Cyp27b1* level and *n* = 8 for calcitriol level (**d**); *n* = 6 mice and *n* = 8 humans (**e**); *n* = 3 and 4 (**f**); *n* = 6 (**g**); *n* = 5 (**i**); *n* = 13 lean and *n* = 11 obese patients (**j**). The assay shown in **h** was repeated six times. Statistical significance was determined using Student's two-tailed unpaired *t*-test (**d**,**e**, right; **f**,**g**,**i**,**j**) or one-way ANOVA with Dunnett's post-hoc test (**e**, left).

Vitamin D suppresses IRF7 expression in young adipocytes

Young and thermogenic adipocytes were deficient in IRF7 and were protected from the adverse IFN-β-inducing effect of cytosolic mtRNA, enabling mtRNA to act as an intracellular signalling molecule. Repression of IRF7 may be thus key to promote the metabolically beneficial effects of mtRNA-mediated signalling in adipocytes. We next aimed to explore potential mechanisms that suppress the expression of IRF7 in young adipocytes.

Our NGS analysis revealed prominent expression of VDR-controlled gene networks in young adipocytes (Fig. 4a), and VDR is known to suppress cytosolic RNA-induced IRF7 expression[53,54] and the IFN response[55,56]. The transcriptional activity of VDR was confirmed by the pattern of VDR-controlled gene expression in young adipocytes (Fig. 4b). For example, the known VDR target *Camp*, encoding

the adipose tissue-enriched antimicrobial peptide cathelicidin[57], was highly expressed in young adipocytes (Fig. 4b). By contrast, the VDR-repressed gene *Coro1a* had a low transcript level in young adipocytes (Fig. 4b). *Coro1a* encodes coronin A1, also known as tryptophan–aspartate-containing coat protein[58]. Foetal adipose tissue accumulates vitamin D before birth[59], and, accordingly, the transcription of vitamin D-metabolizing enzymes favoured the storage of vitamin D3 (Vit-D3) and the synthesis of the potent VDR agonist calcitriol in young adipocytes (Fig. 4b,c).

Adipose tissue of young mice was rich in Vit-D3, and VDR protein expression was higher in young adipose tissue than in its adult counterpart (Fig. 4c). Moreover, cytosolic dsRNA and mtRNA increased transcription of the calcitriol-synthesis gene *Cyp27b1* and enhanced Vit-D3–calcitriol conversion in adipocytes (Fig. 4d). Vit-D3 effectively
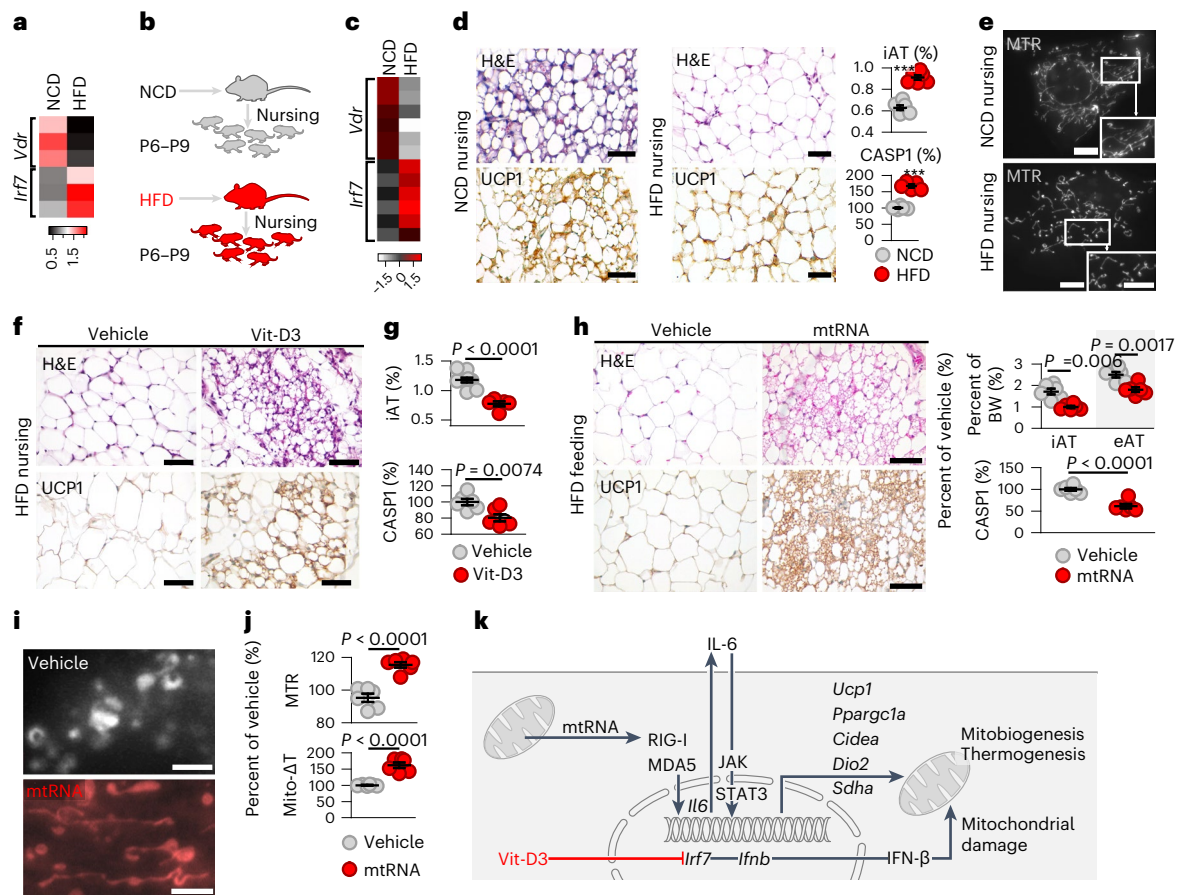
Fig. 5 | Effect of cytosolic mtRNA combined with Vit-D3 treatment on diet-induced obesity. a, Levels of *Vdr* and *Irf7* in inguinal adipose tissue of HFD-fed adult mice. NCD, normal chow diet. **b**, Nursing mice received an HFD or an NCD between postnatal day (P6) and postnatal day 9 (P9) of the offspring. Mice nursed by NCD-fed or HFD-fed dams were analysed at postnatal day 10. **c**, *Vdr* and *Irf7* expression in the inguinal adipose tissue of the offspring. **d**, Left, histology of inguinal adipose tissue (iAT). UCP1, UCP1 immunostaining; scale bar, 50 μm. Note the lack of multilocular adipocytes in mice nursed by HFD-fed dams. Right, ratio of inguinal adipose tissue and body weight, and inflammasome-associated caspase 1 (CASP1) activity of adipocytes. **e**, Mitochondrial network in adipocytes of the offspring. Scale bar, 10 μm. **f**, Mice were nursed by HFD-fed dams and treated with vehicle or Vit-D3 from postnatal day 6 to postnatal day 9. Histology of inguinal adipose tissue on postnatal day 10. Scale bar, 50 μm. **g**, Ratio of inguinal adipose tissue and body weight, and CASP1 activity of adipocytes. **h**, In adult HFD-fed mice, inguinal adipose tissue was transfected with vehicle or 0.6 μg per g body weight (BW) mtRNA for 14 d. Both groups received 4 ng

per g body weight Vit-D3 daily. Histology of inguinal adipose tissue of vehicle- or mtRNA-transfected mice. Adipose tissue weight/body weight ratio and CASP1 activity of adipocytes. eAT, epididymal adipose tissue. **i**, Mitochondrial network of adipocytes isolated from vehicle- or mtRNA-transfected mice. Scale bar, 10 μm. Note the expansion of the mitochondrial network after mtRNA treatment. **j**, Mitochondrial mass (relative MTR fluorescent intensity) and Mito-ΔT in adipocytes isolated from vehicle- or mtRNA-transfected mice. Data are represented as mean ± s.e.m. *n* = 6 (**a**–**d**,**g**,**h**,**j**) biologically independent samples. The assay shown in **d**,**e**,**f**,**h**,**i** was repeated six times. Statistical significance was determined using Student's two-tailed unpaired *t*-test. **k**, Scheme of retrograde mitochondrion-to-nucleus signalling through mtRNA. Cytosolic mtRNA activates IL-6 synthesis, an inducer of thermogenic fat cell differentiation in the newborn, through RIG-I and MDA5. VDR simultaneously suppresses IRF7 expression and abrogates the IFN response to cytosolic mtRNA. The net effect of mtRNA is mitobiogenesis and thermogenesis.

---

suppressed *Irf7* transcription in mouse and human adipocytes (Fig. 4e). This effect was VDR dependent, and inhibition of VDR signalling augmented mtRNA-induced *Ifnb* transcription (Fig. 4f). In turn, Vit-D3 abrogated *Ifnb* expression in mouse adipocytes in response to cytosolic mtRNA (Fig. 4g). This effect of Vit-D3 mimicked that of a potent nuclear factor (NF)-κB inhibitor (Fig. 4g). Similarly, Vit-D3 mitigated IFN-β production in human adult adipocytes in response to cytosolic mtRNA (Fig. 4g).

Obesity in early postnatal life triggers adipocyte IRF7 expression

Inhibition of VDR signalling in young mice led to the loss of beige adipocytes in adipose tissue (Fig. 4h) and increased IRF7 protein levels in adipocytes (Fig. 4i). Paediatric obesity was associated with compromised expression of VDR-controlled gene networks in the adipose tissue of

children and lower expression of *CYP27A1*, which is involved in the initial activation of Vit-D3 (Fig. 4j). These alterations were associated with an increased *IRF7* level (Fig. 2c) and the expression of IRF7-target genes (Fig. 4j). Similarly, diet-induced obesity increased the adipose tissue level of *Irf7* and abrogated *Vdr* expression in mice (Fig. 5a). Altogether, these data show that obesity is linked to deficient VDR signalling, which is further associated with increased IRF7 expression.

We next studied a mouse model of childhood obesity using newborn mice nursed by dams fed a high-fat diet (HFD) (Fig. 5b)[60]. Adipocytes of the offspring of HFD-fed dams had compromised *Vdr* expression and robust *Irf7* expression (Fig. 5c), and beige adipocytes were lacking from their subcutaneous adipose tissue (Fig. 5d). Ultimately, obesity developed in offspring, and adipocytes showed inflammasome activation, a hallmark of adipose tissue inflammation[61] (Fig. 5d). Moreover, the mitochondrial network was compromised in
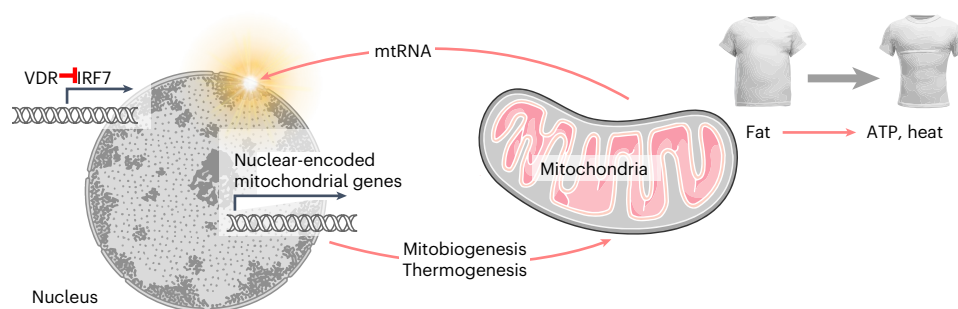
Fig. 6 | Role of mtRNA signalling in young adipocytes. Albeit cytosolic mtRNA is a harmful signal, it can act as a metabolically beneficial mitochondrion-to-nucleus messenger when IRF7 expression is suppressed. VDR is an effective suppressor of IRF7 and abrogates the IFN response to cytosolic mtRNA in young adipocytes. Young adipocytes are hence immune tolerant sites for mitochondria, allowing retrograde mitochondrion-to-nucleus signalling through mtRNA, which is key for mitobiogenesis and beige fat development. See also a Video Summary available in the Supplementary Information.

adipocytes of young mice nursed by HFD-fed dams (Fig. 5e). In turn, Vit-D3 treatment reverted these adverse changes and protected beige adipocyte content in young mice (Fig. 5f), alleviating obesity and adipocyte inflammation (Fig. 5g).

In adult HFD-fed mice, cytosolic delivery of mtRNA into the inguinal adipose tissue depot, combined with Vit-D3 treatment, reduced *Irf7* levels (and not *Irf3* levels) and increased beige adipocyte content (Fig. 5h and Extended Data Fig. 7a), alleviated obesity and adipocyte inflammation and increased mitochondrial mass, thermogenesis and energy expenditure (Fig. 5h–j and Extended Data Figs. 7b,c and 8).

Discussion

Overall, our findings show that, in young adipocytes, cytosolic mtRNA stimulates expression of nuclear-encoded mitochondrial genes and promotes beige adipocyte development through the RIG-I–MDA5–interleukin (IL)-6–signal transducer and activator of transcription (STAT)3 pathway (Fig. 5k). This mitochondrion-to-nucleus signalling is effective when the immune response against cytosolic mtRNA is suppressed by VDR activation and consequently low IRF7 expression in adipocytes (Fig. 5k). These mechanisms protect against obesity by evoking thermogenic potential in adipocytes and promoting thermogenesis from stored fat (Fig. 6, Video Summary in the Supplementary Information).

Adipose tissue inflammation is considered deleterious for metabolism[4,62]; however, multiple lines of evidence implicate IL-6–Janus kinase (JAK)–STAT3 signalling in the differentiation of thermogenic adipose tissue[16,51,52,63,64], and an autocrine IL-6–STAT3 signalling loop is sustained by breast milk-derived lipids in the adipose tissue of newborns[16]. Several inflammatory signalling mechanisms that trigger obesity-associated metabolic impairment also sustain beige adipocytes[35,52,64,65]. Here we report the unexpected finding that beige adipocyte development is promoted by a potentially inflammation-evoking cytosolic RNA signal released by the mitochondria of adipocytes.

The endosymbiotic origin of mitochondria has led to a metabolic co-dependence of mitochondria and host cells[22]. This is driven by bidirectional signalling between the nucleus and the mitochondria, as the majority of genes required for the maintenance of mitochondria are encoded in the nuclear genome. We show that, analogous to a symbiont–host interaction, efflux of mtRNA from the mitochondria activates cytosolic RNA sensors that stimulate an autocrine IL-6–STAT3 signalling loop, ultimately triggering nuclear expression of beige adipocyte genes. Noncoding RNA species of mitochondria are known to increase transcription of mitochondrial genome-encoded genes[66], and noncoding RNA signals are thought to function as mitochondrion-to-nucleus signals[67]. As a comparable mechanism, we show that mtRNA species boost transcription of nuclear genome-encoded genes for mitobiogenesis and thermogenesis. This is key for mitobiogenesis as the necessary proteins are encoded in the nuclear genome[22].

RIG-I and MDA5 are sensors of cytosolic mtRNA. RIG-I detects dsRNA species with or without a 5′-triphosphate end, MDA5 binds uncapped RNA, and RIG-I and MDA5 selectively recognize short and long dsRNA species, respectively[33,34]. Given the prokaryote origin of mitochondria, various mtRNA species such as mitochondrial ribosomal RNA, uncapped mitochondrial mRNA and noncoding mtRNA can potentially stimulate the cytosolic RNA-sensor system[24,33,34]. We found that beige adipocyte gene transcription was stimulated by RIG-I activation using cytosolic poly(dA:dT) and also by MDA5 activation using cytosolic high-molecular-weight poly(I:C) but not with cytosolic single-stranded RNA. Coherently, deficiency in RIG-I and MDA5 signalling in mice compromised mtRNA-mediated beige adipocyte development, abrogated nucleus-encoded SDH-A expression and mitobiogenesis and promoted the loss of beige adipocytes. These findings are in agreement with a recent report showing that mice lacking RIG-I are prone to obesity and obesity-associated insulin resistance[68], despite being protected from the IFN response[68].

However, the excess release of mitochondrial content activates an IFN response, which is detrimental for thermogenic fat development[28,31,69,70], increases mitochondrial permeability[71], augments inflammasome activation and pyroptosis[72], triggers obesity, mitochondrial dysfunction and the mitochondrial pathway of adipocyte apoptosis and may aggravate obesity-associated metabolic diseases[29,30,73,74]. We show here that young adipocytes have suppressed the IFN response to cytosolic mtRNA due to their suppressed IRF7 expression. As IRF7 is an IFN-inducible gene product, this is in agreement with previous findings that suggest that beige adipocytes repress IFN signalling[28] and the expression of ISGs in adipocytes promotes obesity and adipose tissue inflammation[29]. IRF3 and IRF7 are key transcription factors regulating ISGs; however, their role in obesity development is conflicting. Lack of IRF7 protects from diet-induced obesity[43], while IRF3-deficient mice develop obesity spontaneously[75]. We found that *Irf3* expression was similar in adipocytes of young and adult mice, while *Irf7* was minimally expressed in young adipocytes. Similarly, paediatric obesity was associated with increased *IRF7* expression in adipose tissue, without a significant increase in *IRF3* levels. Diet-induced obesity in mice and obesity in children were associated with robust expression of genes encoding IRF7-associated pathways. This is in agreement with findings on increased expression of the IRF7-target genes *AIM2* and *IFI16* in type 2 diabetic obese human adipose tissue[76]. Adipose tissue expansion and obesity are associated with the activation of STAT1 and NF-κB signalling, which may account for the increase in IRF7 expression during postnatal adipocyte development and in obesity[29,64,77].

We also show that suppressed *Irf7* expression and mtRNA-induced *Ifnb* expression were associated with the thermogenic adipocyte phenotype. Inguinal adipocytes of young mice and interscapular brown adipose tissue of adult mice were deficient in IRF7 and were lacking

mtRNA-induced *Ifnb* expression. Interscapular brown adipocytes are strongly thermogenic cells and are descendants of the Myf5+ lineage derived from skeletal muscle progenitors in mice[78–80]. Primates and humans have different thermoregulatory mechanisms than those of small rodents[17], and thermogenic adipocytes of a newborn human are scattered within white fat depots[12]. Equivalents of these cells appear in newborn mice as well[11]. These thermogenic fat cells are unrelated to Myf5+ progenitors, and they develop from progenitors of white fat cells[79]. It appears that thermogenic fat cells in newborn subcutaneous tissue and in adult interscapular adipose tissue have distinct transcriptional profiles and specific developmental programmes[11,81]. Nevertheless, this study shows that, irrespective of their origin and development, thermogenic adipocytes have suppressed IRF7 expression and are eventually lacking an IFN response to cytosolic mtRNA. The IFN response augments inflammasome activation, which further damages mitochondria[71]. However, a gene network encoding inflammasome proteins had suppressed expression in young (thermogenic) adipocytes, suggesting their potential protection from mitochondrion-damaging inflammasome activation. These, in our understanding, favour the expansion of the mitochondrial network and allow mitochondrial thermogenesis.

We show that VDR signalling contributes to the suppression of IRF7 expression in adipocytes and that cytosolic mtRNA stimulates calcitriol synthesis and hence supplies a VDR ligand in young adipocytes. However, as a limitation of this study, we have not explored further the mechanism of *Irf7* suppression in interscapular brown adipose tissue in mice, leaving open the possibility that this unique thermogenic fat depot has a VDR-independent mechanism that suppresses *Irf7* expression.

VDR signalling is involved in the innate immune response in adipose tissue[57], and VDR activation inhibits the inflammasome and the IFN response[53–56,82]. Vit-D3 supplementation is now routine in postnatal care; however, Vit-D3 deficiency is prevalent among obese children and adolescents and is a risk factor for metabolic diseases[83,84]. Vit-D3–VDR signalling is proposed to inhibit weight gain by activating UCP3 in the muscle[85], although VDR overexpression promotes weight gain in mice[86]. Indeed, the promotion of formula feeding originally served to increase the supply of Vit-D3 and induce weight gain[87], but formula lacks the maternal lipid species that maintain beige fat and has obesogenic effects[16]. VDR signalling was impaired in the adipose tissue of obese children; therefore, despite increasing Vit-D3 levels, formula milk is not sufficient to trigger beige adipogenesis. However, when Vit-D3 supplementation is combined with stimulation of cytosolic mtRNA signalling, beige adipocytes develop and obesity is reduced.

In summary, the thermogenic potential of young adipocytes in early postnatal life is dependent on mtRNA-mediated signalling and suppression of the immune response to cytosolic mtRNA. In obesity, adipocytes respond with inflammation to mtRNA, which is unfavourable for the mitochondrial network. Repressing this immune response along with restoring mtRNA-mediated mitochondrion-to-nucleus signalling may represent an effective mechanism to increase beige fat and mitigate obesity.

Methods

Animals and cells
We used WT male C57BL/6 (Charles River Laboratories), *Irf7*−/− (Riken), *Ddx58*−/− and *Mda5*−/− (kindly provided by G. Hartmann, University of Bonn, Germany) mice. Mice were housed under SPF conditions. Animal experiments were approved by local ethics committees. Primary mouse adipocytes were isolated by collagenase digestion and separation of cell fractions and subsequently analysed or cultured, as described previously[16].

Human samples
Subcutaneous adipose tissue (groin region, ischiorectal fossa, abdominal and pectoral fat depots) from human infants, adolescents and young adults was collected in the Leipzig Childhood Adipose Tissue cohort and at the University of Debrecen during elective surgery[2]. For all children included in the study, written informed consent was obtained from parents or guardians, and the study has been conducted in accordance with ethical guidelines of the Declaration of Helsinki. The study protocol was approved by the local ethics committee of the Medical Faculty, University of Leipzig (265-08-ff, NCT02208141) and the University of Debrecen (RKEB 6057 and 6149). Adult adipocyte samples were collected in our previous study[16]. In Fig. 3h,i, we used adipocytes obtained from the groin region.

mRNA analysis and next-generation sequencing
Extraction of total RNA was performed as described previously[11]. qPCR assays were carried out on the Quantabio platform, using *Bactin* (*Actb*), *Gapdh* and *Ppia* as references. Primer sequences are provided in Supplementary Table 1. NGS analysis was carried out on the BGISEQ-500 platform by BGI Genomics, generating about 26.20 million reads per sample (Extended Data Fig. 8). EnrichR, P1nther and Interferome 2.0 were used for annotation of transcripts; clustered image maps (CIMs, heatmaps) were rendered by CIMMiner and Heatmapper. Gene expression in human samples was quantified by Illumina HT-12 v4 Gene Expression BeadChip arrays, and data were background corrected and quantile normalized[11].

Supplementary methods
Cytosolic delivery of mtRNA, ELISA assays, flow cytometry, histology, image analysis and TEM analysis are provided in the Supplementary Information and Extended Data Fig. 8.

Data representation and statistics
Data are represented as mean ± s.e.m., along with each individual data point. When data are represented as CIMs to visualize gene transcription differences between experimental conditions, we indicate fold changes or Z scores of the relative abundance. Statistical tests and significance are indicated in the respective figures.

Reporting summary
Further information on research design is available in the Nature Portfolio Reporting Summary linked to this article.

Data availability
Data are available for secondary use upon request, and key experimental data are accessible via Figshare (https://doi.org/10.6084/m9.figshare.21202400). FlowRepository identifiers of flow cytometry data are as follows: FR-FCM-Z236, FR-FCM-Z2R6, FR-FCM-ZYPU, FR-FCM-ZYUU, FR-FCM-Z5QA. NGS data are deposited at GEO under the accession number GSE185317. For secondary analysis, we used our previously published NGS datasets, with accession numbers GSE125405 and GSE133500. Source data are provided with this paper.

References
1. Geserick, M. et al. Acceleration of BMI in early childhood and risk of sustained obesity. *N. Engl. J. Med.* **379**, 1303–1312 (2018).
2. Landgraf, K. et al. Evidence of early alterations in adipose tissue biology and function and its association with obesity-related inflammation and insulin resistance in children. *Diabetes* **64**, 1249–1261 (2015).
3. Dietz, W. H. Overweight in childhood and adolescence. *N. Engl. J. Med.* **350**, 855–857 (2004).
4. Christ, A. & Latz, E. The Western lifestyle has lasting effects on metaflammation. *Nat. Rev. Immunol.* **19**, 267–268 (2019).
5. Eriksson, J. G., Forsén, T., Tuomilehto, J., Osmond, C. & Barker, D. J. Early adiposity rebound in childhood and risk of type 2 diabetes in adult life. *Diabetologia* **46**, 190–194 (2003).

6. Pietrobelli, A., Agosti, M. & the MeNu, G. Nutrition in the first 1000 days: ten practices to minimize obesity emerging from published science. *Int. J. Environ. Res. Public Health* **14**, 1491 (2017).

7. Rolland-Cachera, M. F. et al. Adiposity rebound in children: a simple indicator for predicting obesity. *Am. J. Clin. Nutr.* **39**, 129–135 (1984).

8. Dietz, W. H. Critical periods in childhood for the development of obesity. *Am. J. Clin. Nutr.* **59**, 955–959 (1994).

9. Siervogel, R. M., Roche, A. F., Guo, S. M., Mukherjee, D. & Chumlea, W. C. Patterns of change in weight/stature2 from 2 to 18 years: findings from long-term serial data for children in the Fels Longitudinal Growth Study. *Int. J. Obes.* **15**, 479–485 (1991).

10. Herrera, E. & Amusquivar, E. Lipid metabolism in the fetus and the newborn. *Diabetes Metab. Res. Rev.* **16**, 202–210 (2000).

11. Hoang, A. C., Yu, H. & Röszer, T. Transcriptional landscaping identifies a beige adipocyte depot in the newborn mouse. *Cells* **10**, 2368 (2021).

12. Rockstroh, D. et al. Direct evidence of brown adipocytes in different fat depots in children. *PLoS ONE* **10**, e0117841 (2015).

13. Sinclair, J. C. *Temperature Regulation and Energy Metabolism in the Newborn* (*Monographs in Neonatology*) (Grune & Stratton, 1978).

14. Persson, B. Carbohydrate and lipid metabolism in the newborn infant. *Acta Anaesthesiol. Scand.* **18**, https://doi.org/10.1111/j.1399-6576.1974.tb00706.x (1974).

15. Hahn, P. in *Perinatal Physiology* (ed Stave, U.) Ch. 19 (Plenum Medical Book Company, 1970).

16. Yu, H. et al. Breast milk alkylglycerols sustain beige adipocytes through adipose tissue macrophages. *J. Clin. Invest.* **129**, 2485–2499 (2019).

17. Lidell, M. E. Brown adipose tissue in human infants. *Handb. Exp. Pharmacol.* **251**, 107–123 (2019).

18. Hahn, P. & Novak, M. Development of brown and white adipose tissue. *J. Lipid Res.* **16**, 79–91 (1975).

19. Ikeda, K., Maretich, P. & Kajimura, S. The common and distinct features of brown and beige adipocytes. *Trends Endocrinol. Metab.* **29**, 191–200 (2018).

20. Boudina, S. & Graham, T. E. Mitochondrial function/dysfunction in white adipose tissue. *Exp. Physiol.* **99**, 1168–1178 (2014).

21. Riley, J. S. & Tait, S. W. Mitochondrial DNA in inflammation and immunity. *EMBO Rep.* **21**, e49799 (2020).

22. Youle, R. J. Mitochondria—striking a balance between host and endosymbiont. *Science* **365**, eaaw9855 (2019).

23. Zhong, Z. et al. New mitochondrial DNA synthesis enables NLRP3 inflammasome activation. *Nature* **560**, 198–203 (2018).

24. Dhir, A. et al. Mitochondrial double-stranded RNA triggers antiviral signalling in humans. *Nature* **560**, 238–242 (2018).

25. Bahat, A., MacVicar, T. & Langer, T. Metabolism and innate immunity meet at the mitochondria. *Front. Cell Dev. Biol.* **9**, 720490 (2021).

26. Ferreira, R. C. et al. A type I interferon transcriptional signature precedes autoimmunity in children genetically at risk for type 1 diabetes. *Diabetes* **63**, 2538–2550 (2014).

27. Ghazarian, M. et al. Type I interferon responses drive intrahepatic T cells to promote metabolic syndrome. *Sci. Immunol.* **2**, eaai7616 (2017).

28. Kissig, M. et al. PRDM16 represses the type I interferon response in adipocytes to promote mitochondrial and thermogenic programing. *EMBO J.* **36**, 1528–1542 (2017).

29. Chan, C. C. et al. Type I interferon sensing unlocks dormant adipocyte inflammatory potential. *Nat. Commun.* **11**, 2745 (2020).

30. Bai, J. & Liu, F. The cGAS–cGAMP–STING pathway: a molecular link between immunity and metabolism. *Diabetes* **68**, 1099–1108 (2019).

31. Bai, J. et al. Mitochondrial stress-activated cGAS–STING pathway inhibits thermogenic program and contributes to overnutrition-induced obesity in mice. *Commun. Biol.* **3**, 257 (2020).

32. Röszer, T. Co-evolution of breast milk lipid signaling and thermogenic adipose tissue. *Biomolecules* **11**, 1705 (2021).

33. Dias Junior, A. G., Sampaio, N. G. & Rehwinkel, J. A balancing act: MDA5 in antiviral immunity and autoinflammation. *Trends Microbiol.* **27**, 75–85 (2019).

34. Kato, H. et al. Length-dependent recognition of double-stranded ribonucleic acids by retinoic acid-inducible gene-I and melanoma differentiation-associated gene 5. *J. Exp. Med.* **205**, 1601–1610 (2008).

35. Alsaggar, M., Mills, M. & Liu, D. Interferon β overexpression attenuates adipose tissue inflammation and high-fat diet-induced obesity and maintains glucose homeostasis. *Gene Ther.* **24**, 60–66 (2017).

36. Wieser, V. et al. Adipose type I interferon signalling protects against metabolic dysfunction. *Gut* **67**, 157–165 (2018).

37. Meyer, A. et al. IFN-β-induced reactive oxygen species and mitochondrial damage contribute to muscle impairment and inflammation maintenance in dermatomyositis. *Acta Neuropathol.* **134**, 655–666 (2017).

38. Shan, B., Vazquez, E. & Lewis, J. Interferon selectively inhibits the expression of mitochondrial genes: a novel pathway for interferon-mediated responses. *EMBO J.* **9**, 4307–4314 (1991).

39. Ablasser, A. et al. RIG-I-dependent sensing of poly(dA:dT) through the induction of an RNA polymerase III-transcribed RNA intermediate. *Nat. Immunol.* **10**, 1065–1072 (2009).

40. Honda, K., Takaoka, A. & Taniguchi, T. Type I inteferon gene induction by the interferon regulatory factor family of transcription factors. *Immunity* **25**, 349–360 (2006).

41. Ning, S., Pagano, J. S. & Barber, G. N. IRF7: activation, regulation, modification and function. *Genes Immun.* **12**, 399–414 (2011).

42. Honda, K. et al. IRF-7 is the master regulator of type-I interferon-dependent immune responses. *Nature* **434**, 772–777 (2005).

43. Wang, X. A. et al. Interferon regulatory factor 7 deficiency prevents diet-induced obesity and insulin resistance. *Am. J. Physiol. Endocrinol. Metab.* **305**, E485–E495 (2013).

44. Motwani, M., Pesiridis, S. & Fitzgerald, K. A. DNA sensing by the cGAS–STING pathway in health and disease. *Nat. Rev. Genet.* **20**, 657–674 (2019).

45. Takaoka, A. et al. DAI (DLM-1/ZBP1) is a cytosolic DNA sensor and an activator of innate immune response. *Nature* **448**, 501–505 (2007).

46. Shin, S.-I. et al. Z-DNA-forming sites identified by ChIP–seq are associated with actively transcribed regions in the human genome. *DNA Res.* **23**, 477–486 (2016).

47. Lugrin, J. & Martinon, F. The AIM2 inflammasome: sensor of pathogens and cellular perturbations. *Immunol. Rev.* **281**, 99–114 (2018).

48. Unterholzner, L. et al. IFI16 is an innate immune sensor for intracellular DNA. *Nat. Immunol.* **11**, 997–1004 (2010).

49. Sugimoto, S. et al. Brown adipose tissue-derived MaR2 contributes to cold-induced resolution of inflammation. *Nat. Metab.* **4**, 775–790 (2022).

50. Moon, J. et al. Brown adipose tissue ameliorates autoimmune arthritis via inhibition of T_H17 cells. *Sci. Rep.* **10**, 12374 (2020).

51. Babaei, R. et al. Jak–TGFβ cross-talk links transient adipose tissue inflammation to beige adipogenesis. *Sci. Signal.* **11**, eaai7838 (2018).

52. Kristóf, E. et al. Interleukin-6 released from differentiating human beige adipocytes improves browning. *Exp. Cell Res.* **377**, 47–55 (2019).

53. Teymoori-Rad, M., Shokri, F., Salimi, V. & Marashi, S. M. The interplay between vitamin D and viral infections. *Rev. Med. Virol.* **29**, e2032 (2019).

54. Stoppelenburg, A. J., von Hegedus, J. H., Huis in't Veld, R., Bont, L. & Boes, M. Defective control of vitamin D receptor-mediated epithelial STAT1 signalling predisposes to severe respiratory syncytial virus bronchiolitis. *J. Pathol.* **232**, 57–64 (2014).

55. Rao, Z. et al. Vitamin D receptor inhibits NLRP3 activation by impeding its BRCC3-mediated deubiquitination. *Front. Immunol.* **10**, 2783 (2019).

56. Nakajo, T., Katayoshi, T., Kitajima, N. & Tsuji-Naito, K. 1,25-dihydroxyvitamin D3 attenuates IL-1β secretion by suppressing NLRP1 inflammasome activation by upregulating the NRF2–HO-1 pathway in epidermal keratinocytes. *Redox Biol.* **48**, 102203 (2021).

57. Zhang, L. J. et al. Innate immunity. Dermal adipocytes protect against invasive *Staphylococcus aureus* skin infection. *Science* **347**, 67–71 (2015).

58. Seto, S., Tsujimura, K. & Koide, Y. Coronin-1a inhibits autophagosome formation around *Mycobacterium tuberculosis*-containing phagosomes and assists mycobacterial survival in macrophages. *Cell. Microbiol.* **14**, 710–727 (2012).

59. Tare, M., Parkington, H. C. & Morley, R. in *Early Life Origin of Health and Disease* (eds Wintour, E. M. & Owens, J. A.) (Springer, 2006).

60. Masuyama, H. & Hiramatsu, Y. Additive effects of maternal high fat diet during lactation on mouse offspring. *PLoS ONE* **9**, e92805 (2014).

61. Vandanmagsar, B. et al. The NLRP3 inflammasome instigates obesity-induced inflammation and insulin resistance. *Nat. Med.* **17**, 179–188 (2011).

62. Villarroya, F., Cereijo, R., Gavaldà-Navarro, A., Villarroya, J. & Giralt, M. Inflammation of brown/beige adipose tissues in obesity and metabolic disease. *J. Intern. Med.* **284**, 492–504 (2018).

63. Derecka, M. et al. Tyk2 and Stat3 regulate brown adipose tissue differentiation and obesity. *Cell Metab.* **16**, 814–824 (2012).

64. Asterholm, I. W. et al. Adipocyte inflammation is essential for healthy adipose tissue expansion and remodeling. *Cell Metab.* **20**, 103–118 (2014).

65. Cao, W. et al. p38 mitogen-activated protein kinase is the central regulator of cyclic AMP-dependent transcription of the brown fat uncoupling protein 1 gene. *Mol. Cell. Biol.* **24**, 3057–3067 (2004).

66. Ro, S. et al. The mitochondrial genome encodes abundant small noncoding RNAs. *Cell Res.* **23**, 759–774 (2013).

67. Vendramin, R., Marine, J. C. & Leucci, E. Non-coding RNAs: the dark side of nuclear–mitochondrial communication. *EMBO J.* **36**, 1123–1133 (2017).

68. Yang, G. et al. RIG-I deficiency promotes obesity-induced insulin resistance. *Pharmaceuticals* **14**, 1178 (2021).

69. Kumari, M. et al. IRF3 promotes adipose inflammation and insulin resistance and represses browning. *J. Clin. Invest.* **126**, 2839–2854 (2016).

70. Yan, S. et al. IRF3 reduces adipose thermogenesis via ISG15-mediated reprogramming of glycolysis. *J. Clin. Invest.* **131**, e144888 (2021).

71. Rogers, C. et al. Gasdermin pores permeabilize mitochondria to augment caspase-3 activation during apoptosis and inflammasome activation. *Nat. Commun.* **10**, 1689 (2019).

72. Labzin, L. I., Lauterbach, M. A. & Latz, E. Interferons and inflammasomes: cooperation and counterregulation in disease. *J. Allergy Clin. Immunol.* **138**, 37–46 (2016).

73. Gkirtzimanaki, K. et al. IFNα impairs autophagic degradation of mtDNA promoting autoreactivity of SLE monocytes in a STING-dependent fashion. *Cell Rep.* **25**, 921–933 (2018).

74. Birk, R. Z. & Rubinstein, M. IFN-α induces apoptosis of adipose tissue cells. *Biochem. Biophys. Res. Commun.* **345**, 669–674 (2006).

75. Tang, P. & Zhang, Y. Regulatory function of interferon regulatory factor 3 in obesity, inflammation and insulin resistance (HUM7P.287). *J. Immunol.* **192**, 184.4 (2014).

76. Minchenko, D. The expression of *DDX58*, *IFIH1*, *IFI16*, and *AIM2* genes in obese adolescents and men with insulin resistance. *Sovremennaya Pediatriya* **7**, 106–111 (2017).

77. Berg, A. H., Lin, Y., Lisanti, M. P. & Scherer, P. E. Adipocyte differentiation induces dynamic changes in NF-κB expression and activity. *Am. J. Physiol. Endocrinol. Metab.* **287**, E1178–E1188 (2004).

78. Seale, P. et al. PRDM16 controls a brown fat/skeletal muscle switch. *Nature* **454**, 961–967 (2008).

79. Shan, T. et al. Distinct populations of adipogenic and myogenic Myf5-lineage progenitors in white adipose tissues. *J. Lipid Res.* **54**, 2214–2224 (2013).

80. Sanchez-Gurmaches, J. & Guertin, D. A. Adipocyte lineages: tracing back the origins of fat. *Biochim. Biophys. Acta* **1842**, 340–351 (2014).

81. Cannon, B., de Jong, J. M. A., Fischer, A. W., Nedergaard, J. & Petrovic, N. Human brown adipose tissue: classical brown rather than brite/beige. *Exp. Physiol.* **105**, 1191–1200 (2020).

82. Cippitelli, M. & Santoni, A. Vitamin D3: a transcriptional modulator of the interferon-γ gene. *Eur. J. Immunol.* **28**, 3017–3030 (1998).

83. de Oliveira, L. F., de Azevedo, L. G., da Mota Santana, J., de Sales, L. P. C. & Pereira-Santos, M. Obesity and overweight decreases the effect of vitamin D supplementation in adults: systematic review and meta-analysis of randomized controlled trials. *Rev. Endocr. Metab. Disord.* **21**, 67–76 (2020).

84. Pramono, A., Jocken, J. W. E. & Blaak, E. E. Vitamin D deficiency in the aetiology of obesity-related insulin resistance. *Diabetes Metab. Res. Rev.* **35**, e3146 (2019).

85. Fan, Y. et al. Vitamin D3/VDR resists diet-induced obesity by modulating UCP3 expression in muscles. *J. Biomed. Sci.* **23**, 56–56 (2016).

86. Xu, Y., Lou, Y. & Kong, J. VDR regulates energy metabolism by modulating remodeling in adipose tissue. *Eur. J. Pharmacol.* **865**, 172761 (2019).

87. Biggs, K. et al. Formula milk supplementation on the postnatal ward: a cross-sectional analytical study. *Nutrients* **10**, 608 (2018).

88. Narvaez, C. J., Matthews, D., Broun, E., Chan, M. & Welsh, J. Lean phenotype and resistance to diet-induced obesity in vitamin D receptor knockout mice correlates with induction of uncoupling protein-1 in white adipose tissue. *Endocrinology* **150**, 651–661 (2009).

89. Lorenz, R. et al. ViennaRNA package 2.0. *Algorithms Mol. Biol.* **6**, 26 (2011).

90. Karikó, K., Buckstein, M., Ni, H. & Weissman, D. Suppression of RNA recognition by Toll-like receptors: the impact of nucleoside modification and the evolutionary origin of RNA. *Immunity* **23**, 165–175 (2005).

91. Bakker, P. et al. TLR9 mediates remote liver injury following severe renal ischemia reperfusion. *PLoS ONE* **10**, e0137511 (2015).

92. Lin, R., Mamane, Y. & Hiscott, J. Multiple regulatory domains control IRF-7 activity in response to virus infection. *J. Biol. Chem.* **275**, 34320–34327 (2000).

93. Szklarczyk, D. et al. STRING v11: protein–protein association networks with increased coverage, supporting functional discovery in genome-wide experimental datasets. *Nucleic Acids Res.* **47**, D607–D613 (2019).

94. Luan, Y., Lengyel, P. & Liu, C.-J. p204, a p200 family protein, as a multifunctional regulator of cell proliferation and differentiation. *Cytokine Growth Factor Rev.* **19**, 357–369 (2008).

95. Bourette, R. P. & Mouchiroud, G. The biological role of interferon-inducible P204 protein in the development of the mononuclear phagocyte system. *Front. Biosci.* **13**, 879–886 (2008).

96. Choubey, D. & Panchanathan, R. Interferon-inducible *Ifi200*-family genes in systemic lupus erythematosus. *Immunol. Lett.* **119**, 32–41 (2008).

97. Ampem, G. & Röszer, T. in *Nuclear Receptors: Methods and Experimental Protocols* (ed Badr, M. Z.) 225–236 (Springer, 2019).

98. Vishvanath, L. et al. Pdgfrβ⁺ mural preadipocytes contribute to adipocyte hyperplasia induced by high-fat-diet feeding and prolonged cold exposure in adult mice. *Cell Metab.* **23**, 350–359 (2015).

99. Rhee, M., Kim, J. W., Lee, M. W., Yoon, K. H. & Lee, S. H. Preadipocyte factor 1 regulates adipose tissue browning via TNF-α-converting enzyme-mediated cleavage. *Metabolism* **101**, 153977 (2019).

100. Hepler, C., Vishvanath, L. & Gupta, R. K. Sorting out adipocyte precursors and their role in physiology and disease. *Genes Dev.* **31**, 127–140 (2017).

101. Gao, Z., Daquinag, A. C., Su, F., Snyder, B. & Kolonin, M. G. PDGFRα/PDGFRβ signaling balance modulates progenitor cell differentiation into white and beige adipocytes. *Development* **145**, dev155861 (2018).

102. Tseng, Y. H. et al. Prediction of preadipocyte differentiation by gene expression reveals role of insulin receptor substrates and necdin. *Nat. Cell Biol.* **7**, 601–611 (2005).

103. Seale, P. et al. Transcriptional control of brown fat determination by PRDM16. *Cell Metab.* **6**, 38–54 (2007).

104. Jespersen, N. Z. et al. A classical brown adipose tissue mRNA signature partly overlaps with brite in the supraclavicular region of adult humans. *Cell Metab.* **17**, 798–805 (2013).

105. Kozak, L. P. The genetics of brown adipocyte induction in white fat depots. *Front. Endocrinol.* **2**, 64 (2011).

106. Nascimento, E. B. M. et al. Genetic markers of brown adipose tissue identity and in vitro brown adipose tissue activity in humans. *Obesity* **26**, 135–140 (2018).

107. Perugini, J. et al. Zic1 mRNA is transiently upregulated in subcutaneous fat of acutely cold-exposed mice. *J. Cell. Physiol.* **234**, 2031–2036 (2019).

108. Pilkington, A.-C., Paz, H. A. & Wankhade, U. D. Beige adipose tissue identification and marker specificity—overview. *Front. Endocrinol.* **12**, 599134 (2021).

109. Carobbio, S., Rosen, B. & Vidal-Puig, A. Adipogenesis: new insights into brown adipose tissue differentiation. *J. Mol. Endocrinol.* **51**, T75–T85 (2013).

110. Lee, K.-H. & Kim, N. H. Differential expression of adipocyte-related molecules in the distal epididymal fat of mouse during postnatal period. *Dev. Reprod.* **23**, 213–221 (2019).

111. Taguchi, K. et al. Role of small proliferative adipocytes: possible beige cell progenitors. *J. Endocrinol.* **245**, 65–78 (2020).

112. Hornung, V. et al. 5′-triphosphate RNA is the ligand for RIG-I. *Science* **314**, 994–997 (2006).

113. Waqas, S. F. H. et al. Adipose tissue macrophages develop from bone marrow-independent progenitors in *Xenopus laevis* and mouse. *J. Leukoc. Biol.* **102**, 845–855 (2017).

Acknowledgements

Author contributions

A.C.H., L.S.-S., T.P., V.D. and K.L. carried out experiments; A.K., A.H. and T.S. designed experiments; T.R. conceived the project, designed experiments and wrote the manuscript.

Funding

Competing interests

The authors declare no competing interests.

Additional information

Extended data is available for this paper at https://doi.org/10.1038/s42255-022-00683-w.

Supplementary information The online version contains supplementary material available at https://doi.org/10.1038/s42255-022-00683-w.

Correspondence and requests for materials should be addressed to Tamás Röszer.

Peer review information *Nature Metabolism* thanks the anonymous reviewers for their contribution to the peer review of this work. Primary Handling Editor: Isabella Samuelson, in collaboration with the *Nature Metabolism* team

Reprints and permissions information is available at www.nature.com/reprints.
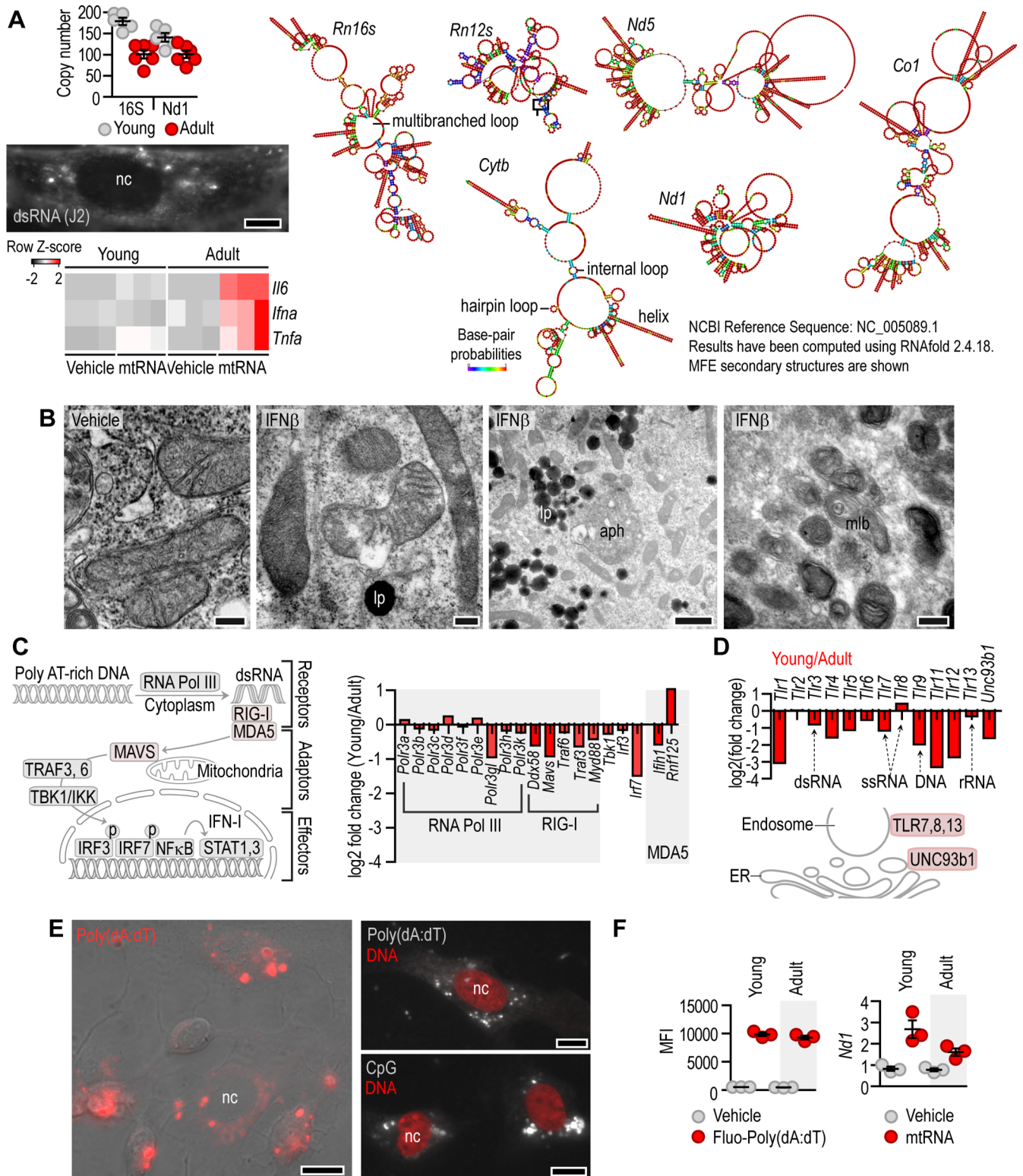
Publisher's note Springer Nature remains neutral with regard to jurisdictional claims in published maps and institutional affiliations.

A

Copy number — Young (grey), Adult (red); 16S, Nd1

dsRNA (J2), nc

Row Z-score −2 to 2; Young / Adult; Il6, Ifna, Tnfa; Vehicle mtRNA Vehicle mtRNA

Rn16s — multibranched loop
Rn12s
Nd5
Co1
Cytb — internal loop
Nd1
hairpin loop — helix
Base-pair probabilities

NCBI Reference Sequence: NC_005089.1
Results have been computed using RNAfold 2.4.18.
MFE secondary structures are shown

B

Vehicle | IFNβ — lp | IFNβ — lp, aph | IFNβ — mlb

C

Poly AT-rich DNA → RNA Pol III → dsRNA (Cytoplasm); RIG-I / MDA5 (Receptors)
TRAF3, 6 ← MAVS → Mitochondria (Adaptors)
TBK1/IKK
IRF3 (p) IRF7 (p) NFκB STAT1,3 → IFN-I (Effectors)

log2 fold change (Young/Adult):
Polr3a, Polr3b, Polr3c, Polr3d, Polr3f, Polr3e, Polr3gl, Polr3h, Polr3k (RNA Pol III); *Ddx58, Mavs, Traf3, Traf6, Myd88, Tbk1, Irf3, Irf7* (RIG-I); *Ifih1, Rnf125* (MDA5)

D

Young/Adult
log2(fold change): *Tlr1, Tlr2, Tlr3, Tlr4, Tlr5, Tlr6, Tlr7, Tlr8, Tlr9, Tlr11, Tlr12, Tlr13, Unc93b1*
dsRNA, ssRNA, DNA, rRNA

Endosome — TLR7,8,13
ER — UNC93b1

E

Poly(dA:dT), nc
Poly(dA:dT) / DNA, nc
CpG / DNA, nc

F

MFI — Young, Adult; Vehicle (grey), Fluo-Poly(dA:dT) (red)
Nd1 — Young, Adult; Vehicle (grey), mtRNA (red)

**Extended Data Fig. 1 | See next page for caption.**

Extended Data Fig. 1 | Recognition of cytosolic mtRNA in adipocytes. (**A**) *Top Left:* Copy number of mtDNA species in adipocytes of young and adult mice, N = 6 biologically independent samples. *Middle Left:* Immunostaining of dsRNA using J2 antibody in mouse adipocyte. nc: nucleus, Scale 10 μm. Assay was repeated three times. *Bottom Left:* Heat map of IFN-response genes in young and adult adipocytes transfected with vehicle or mtRNA (2 μg/ml, 18 h), N = 3 biologically independent samples. 80% confluent mouse adipocytes released 125 ± 20 IU/ml IFNβ in 4 h following mtRNA transfection. *Right:* Predicted minimum free energy (MFE) secondary structures of mtRNA species. Results were computed using ViennaRNA Package 2.0 and RNAfold 2.2.18, as described[88,89]. (**B**) Transmission electron microscopy of mitochondria, also shown in Fig. 1d. Assay repeated six times. Cells were treated with vehicle or IFNβ. lp: lipid droplet, aph:

autophagosome, mlb: multilayered bodies. Scales from left to right: 1 μm, 20 nm, 1 μm, 1 μm. (**C**) Scheme of RIG-I/MDA5 signaling. RNA Pol III: RNA polymerase III, which can generate dsRNA from DNA templates, ultimately activating the RIG-I/MDA5 pathway. *Right:* Expression of RNA Pol III and RIG-I/MDA5 pathway genes in the adipose tissue of young mice. (**D**) *Mitochondrial RNA* stimulates human TLR8 (ref. [90]) and triggers inflammation in mouse macrophages via TLR9 (ref. [91]). Levels of *Tlr8* and *Tlr9* in young and adult subcutaneous adipose tissue in mouse. (**E**) Transfection of mouse adipocytes with rhodamine-conjugated poly (dA:dT) or CpG (a synthetic DNA sequence). Scale bar: 10 μm. Assay was repeated three times. (**F**) Mean fluorescence intensity of rhodamine-conjugated poly (dA:dT) in transfected cells, N = 3 biologically independent samples. Data are represented as mean ± SEM. Relative expression of mitochondrial *Nd1* in transfected cells.
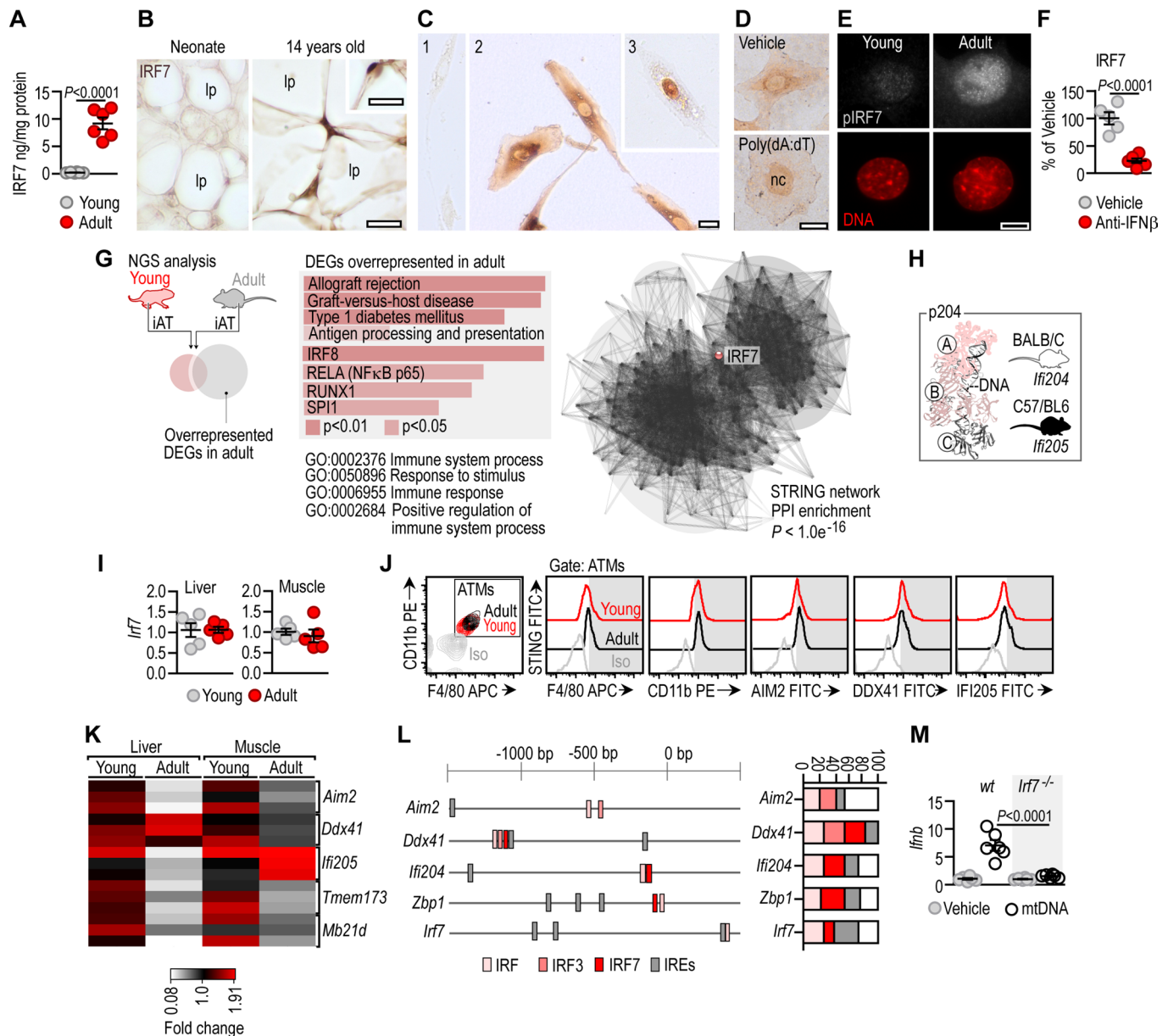
Extended Data Fig. 2 | IRF7-controlled gene networks in mouse adipocytes.
(**A**) Protein level of IRF7 in young and adult mouse adipocytes, determined with ELISA. N = 6 biologically independent samples. (**B**) Immunostaining of IRF7 in the subcutaneous adipose tissue of a human male neonate and a 14 years old male child. Scale 25 μm. lp: lipid droplet. Note the lack of staining in the infant sample, and the robust cytosolic staining in the 14 years old child. Insert shows nucleus associated IRF7 labeling. Assay repeated two times. (**C**) IRF7 immunostaining of *in vitro* cultured adipocytes of a human infant [1] and adolescents [2-3]. Note the lack of staining in the infant adipocytes. IRF7 was detectable in the cytoplasm [2] and rarely in the nuclei [3] of adipocytes from adolescents. Scale 50 μm. (**D**) IRF7 staining of murine adipocytes transfected with vehicle or 5 μg/ml poly(dA:dT) for 1 h. Note the enrichment of IRF7 in the nucleus of poly(dA:dT)-stimulated adipocytes, and indicative of IRF7 activation[41,92]. Scale 25 μm. Assay repeated six times. (**E**) Localization of Ser477-phosphorylated IRF7 in young and adult murine adipocytes, stimulated with 5 μg/ml poly(dA:dT) for 1 h. Scale 10 μm. (**F**) Level of IRF7 (determined with FACS analysis) in murine adipocytes treated with an antibody against IFNβ for 3 h. N = 5 biologically independent samples. (**G**) Scheme of NGS analysis. For RNA sequencing we obtained inguinal fat depots (iAT) of 3-3 mice at postnatal day 6 (young) and at week 8 (adult) and compared

their transcriptional profiles. Gene ontology of differentially-expressed genes (DEGs) overrepresented in adults[93]. Protein-protein association network of DEGs overrepresented in adults. The position of IRF7 within the network is highlighted. (**H**) Structure of the DNA-sensor p204 (IFI204). The three DNA-binding domains are labeled A, B and C. p204 is encoded by *Ifi204* in BALB/C mice. In C57/BL6, however, *Ifi204* has a frameshift mutation and its function is taken over by *Ifi205* (refs. [94–96]). In 3T3-L1 cells, which have a BALB/C origin, we measured *Ifi204*, whereas we measured *Ifi205* in adipocytes from C57/BL6 mice. (**I**) Level of *Irf7* in liver and quadriceps muscle of young and adult mice, N = 5 biologically independent samples. (**J**) FACS plot of ATMs from iAT. ATMs were defined as F4/80⁺, CD11b⁺. FACS analysis of IRF7-associated gene products of young and adult ATMs. Assay was repeated three times. Gating strategy is provided in ref. [97]. (**K**) Expression of *Aim2, Ddx41, Ifi205, Tmem173* and *Mb21d1* in various organs. N = 3 biologically independent samples (**L**) Relative position and percentage of transcription factor binding sites in the promoters of IRF7-target genes. (**M**) Level of *Ifnb* mRNA in *wt* and *Irf7⁻/⁻* adipocytes following mtRNA transfection, N = 6 biologically independent samples. Data are represented as mean ± SEM. Statistical significance was determined using Student's 2-tailed unpaired *t*-test.
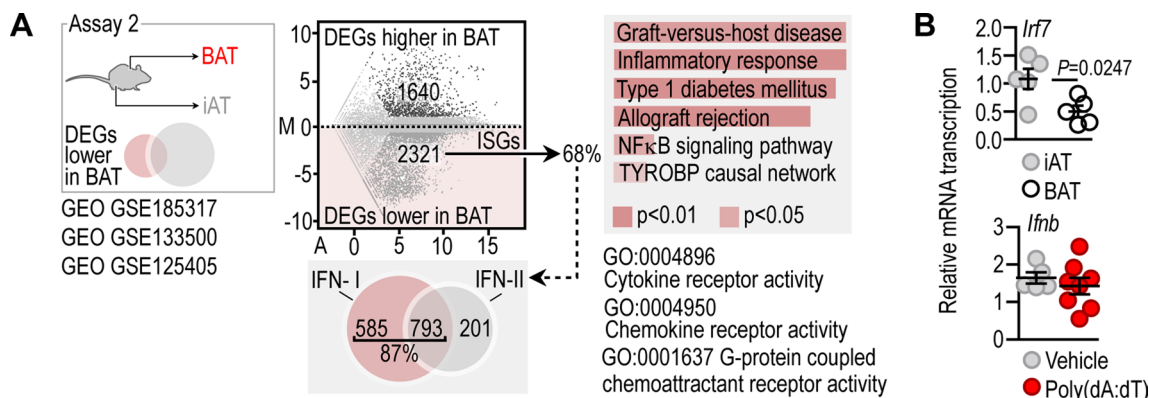
**Extended Data Fig. 3 | IRF7 expression in the brown adipose tissue in mouse.** (**A**) Scheme of NGS analysis in adult mice. Replicate NGS analysis is available in ref. [11]. iAT: inguinal adipose tissue, BAT: interscapular brown adipose tissue. DEGs underrepresented in BAT, and their gene ontology analysis (**B**) *Top:* Comparison of *Irf7* mRNA level in iAT and BAT. *Bottom: Ifnb* level in BAT transfected with vehicle of poly(dA:dT) for 18 h. N = 5 (*Top*) and N = 8 (*Bottom*) biologically independent samples.
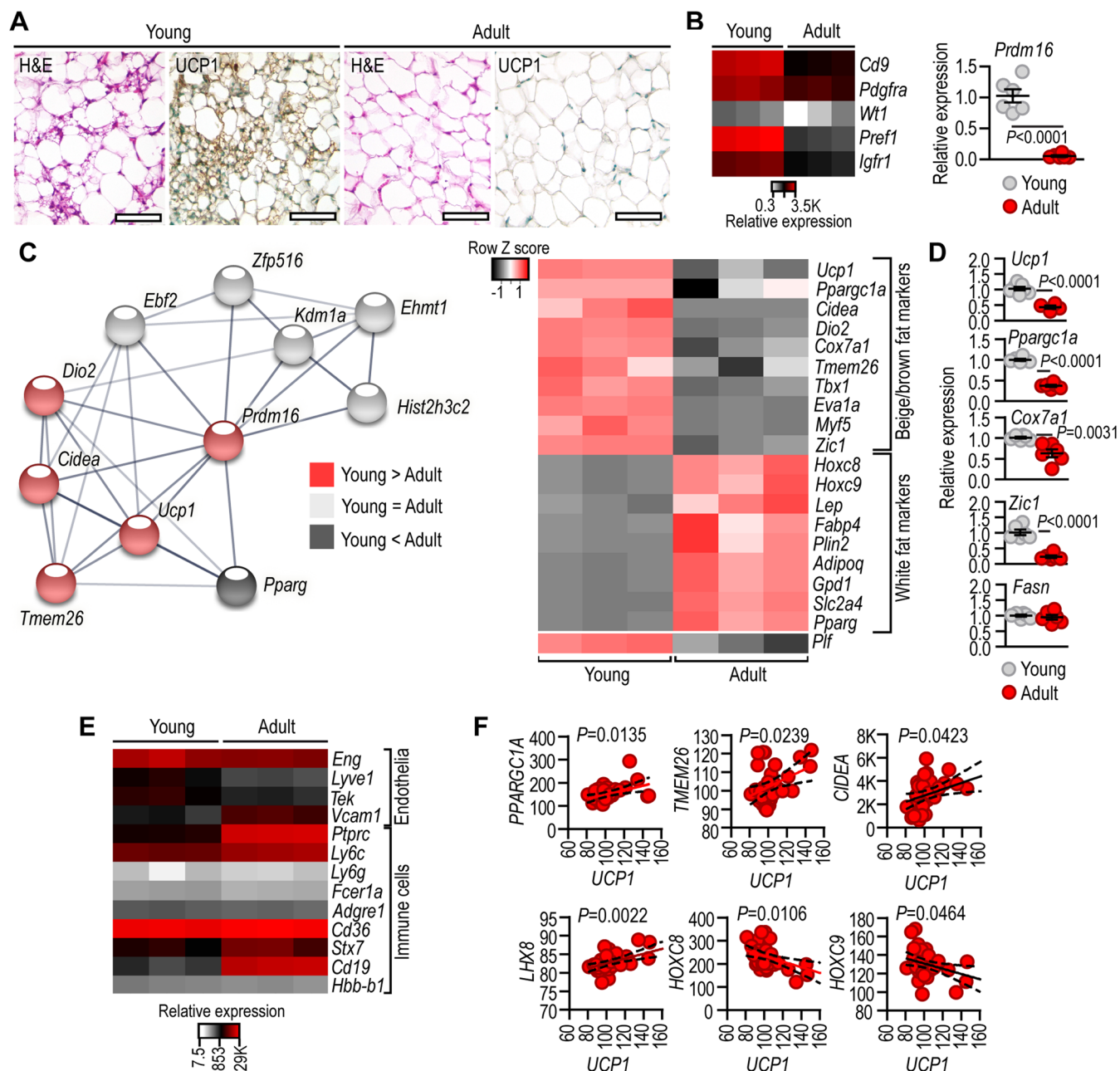
**Extended Data Fig. 4 | Characterization of young and adult adipose tissue.**
(**A**) Hematoxylin and eosin (H&E) staining, and immunostaining of UCP1 in mouse inguinal adipose tissue (iAT) of young and adult mice. Scale: 50 μm, also see further images of these samples in ref. [11]. Assay was repeated six times for both age groups. (**B**) *Left:* Transcription of adipocyte progenitor genes in iAT. N = 3 biologically independent samples. *Pdgfra* and *Pref1* are associated with beige progenitors[98–101]; *Wt1* is a hallmark of epidydimal fat, and is lacking from iAT[102]. *Right:* Adipocyte transcription of *Prdm16*, a key regulator of thermogenic adipocyte development[28,78,103]. (**C**) Gene network associated with PRDM16 in young and adult mouse adipocytes. Red symbols indicate differentially expressed genes (DEGs) overrepresented in young adipocytes. Heat map summarizing the transcription level of beige/brown adipocyte marker genes and white adipocyte marker genes in young and adult iAT. N = 3 biologically independent samples. *Ucp1* is necessary for thermogenesis; *Ppargc1a* for mitochondrial biogenesis; *Cidea, Cox7a1, Dio2, Zic1* are associated with brown/beige adipocytes; *Tmem26* and *Tbx1* are beige adipocyte markers; *Eva1a* is

a brown adipocyte marker[104–109]; *Myf5* is expressed by progenitors of brown adipocytes[80]. Levels of *Hoxc8* and *Hoxc9* increase along white adipocyte development[104], although *Hoxc9* may also be a marker of beige adipocytes[109]. *Lep, Fabp4, Plin2, Adipoq, Gpd1, Slc2a4* and *Pparg* are associated with white adipocyte maturation[110]. *Plf* is expressed by small proliferating preadipocytes with a strong potential to develop into beige adipocytes[111]. (**D**) Expression levels of beige adipocyte genes and *Fasn* (encoding fatty acid synthase) in P6 and P56 adipocytes. N = 6 biologically independent samples. Data are represented as mean ± SEM. Statistical significance was determined using Student's 2-tailed unpaired *t*-test. (**E**) Expression levels of endothelial and immune cell marker genes in young and adult iAT. N = 3 biologically independent samples (**F**) Correlation of *UCP1* levels with beige/brown adipocyte-associated transcripts (*PPARGC1A, TMEM26, CIDEA, LHX8*) and white adipocyte markers (*HOXC8, HOXC9*) in the subcutaneous adipose tissue of human male infants[12,104], each data point represents one donor. *P*-values were determined with linear regression analysis. Age 0.2–3.5 years. Further details in refs. [11,12,16,103,104].
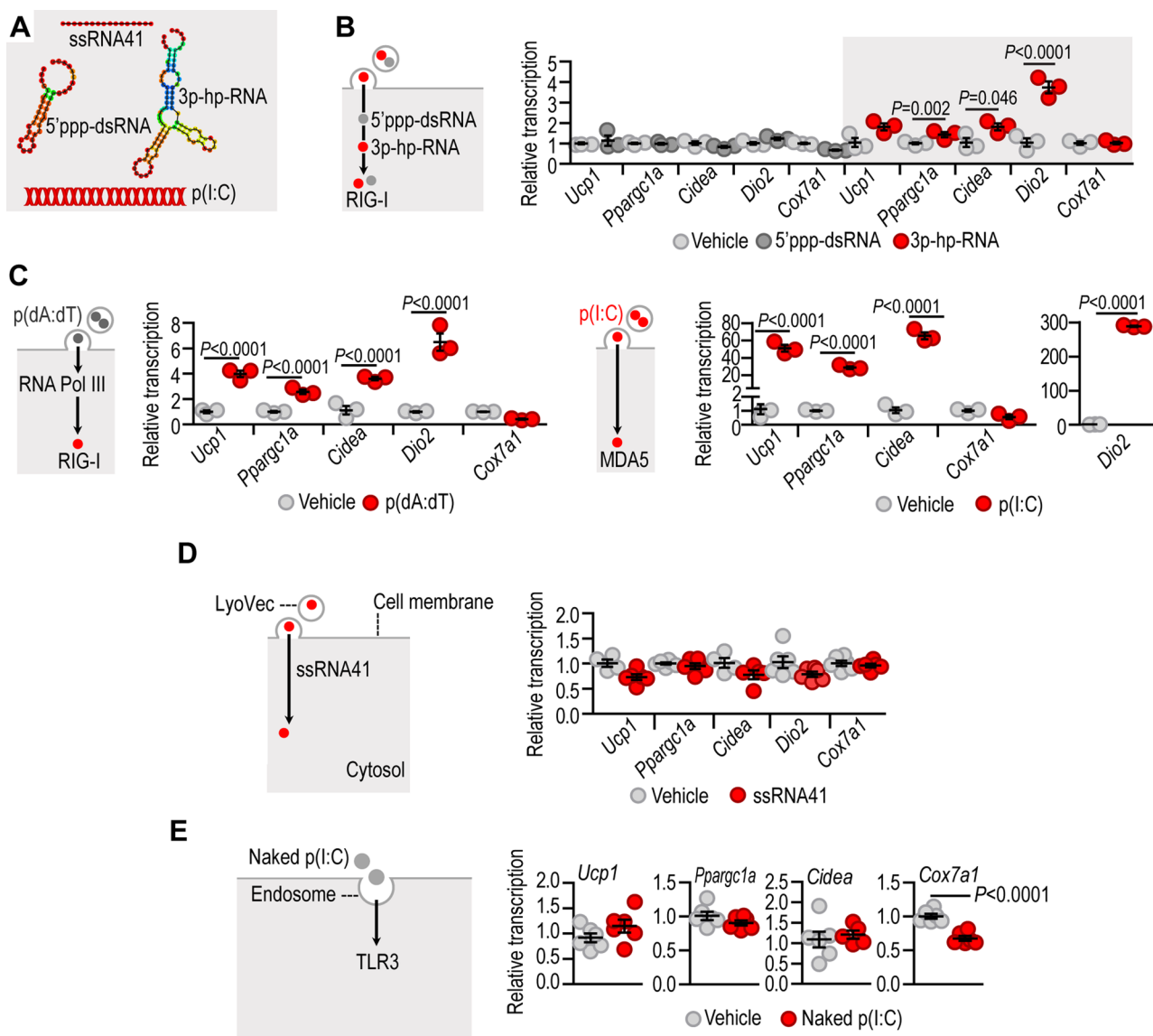
Extended Data Fig. 5 | Effect of RIG-I and MDA5 ligands on beige adipocyte gene expression. (**A**) Secondary and schematic structures of the synthetic ligands used to activate cytosolic RNA sensors. ssRNA41: single-stranded RNA, 3p-hp-RNA: 5′ triphosphate hairpin RNA, is an RIG-I ligand[112], 5′ppp-dsRNA: 5′ triphosphate dsRNA, a ligand for RIG-I, cytosolic p(I:C) activates MDA5 and RIG-I[34], and cytosolic p(dA:dT) is transcribed into RNA and ultimately activates RIG-I[39]. (**B**,**C**) Adipocytes were transfected with RIG-I/MDA5 ligands: 5′ppp-dsRNA, 3p-hairpin-RNA, poly(dA:dT) and poly(I:C) in LyoVec. Levels of beige marker genes was measured 18 h after transfection. N = 3 biologically

independent samples. (**D**) Adipocytes were transfected with 2 µg/ml ssRNA41 using the LyoVec transfection system for cytosol delivery. Levels of beige marker genes was measured 18 h after transfection. N = 6 biologically independent samples. (**E**) 3T3-L1 cells were treated with 5 µg/ml naked poly(I:C) to stimulate TLR3 and beige adipocyte gene transcription was then measured 18 h after treatment. N = 8 biologically independent samples. Data are represented as mean ± SEM. Statistical significance was determined using Student's 2-tailed unpaired *t*-test.
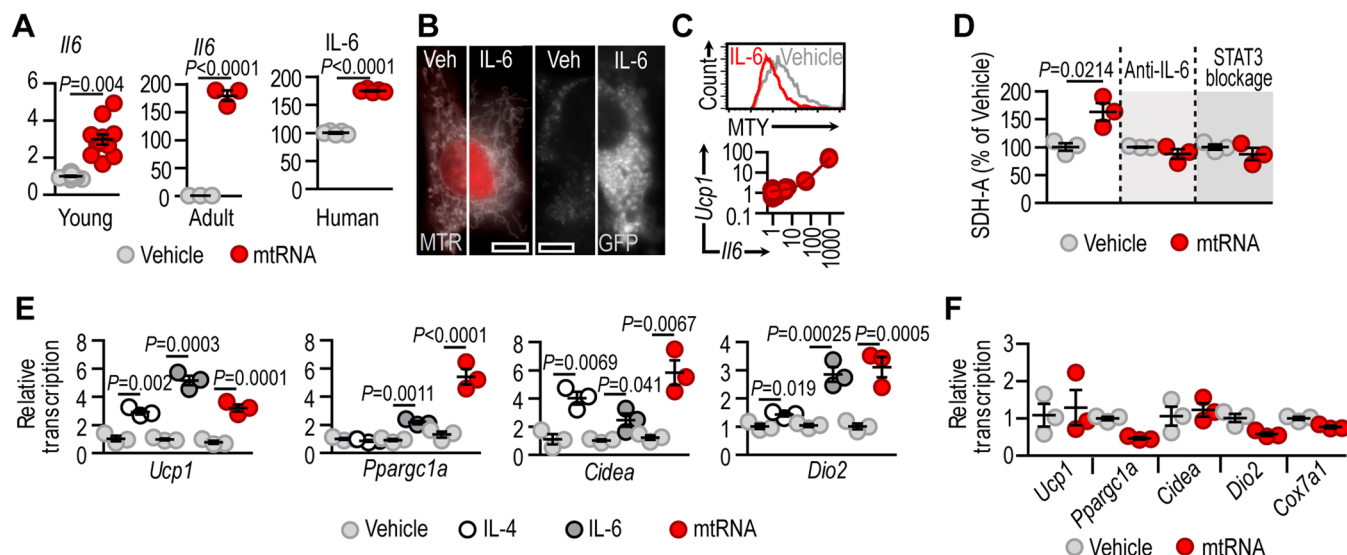
Extended Data Fig. 6 | Effect of IL-6 on beige adipocyte gene expression. (A) *Left and Middle:* Expression of *Il6* mRNA in young and adult mouse adipocytes transfected with mtRNA for 18 h (N = 8, N = 3 biologically independent samples, respectively). *Right:* Level of IL-6 protein in mtRNA-transfected human adipocytes. N = 6 biologically independent samples. **(B)** Effect of 200 pg/ml IL-6 on the amount of newly synthesized (GFP-expressing) mitochondria in mouse adipocytes. Newly formed mitochondria were labeled with the BacMam-GFP transfection system. Scale: 50 μm. Assay was repeated three times. **(C)** Effect of 200 pg/ml IL-6 on the Mitothermo-Yellow (MTY) signal in 3T3-L1 cells. Assay was repeated three times. Correlation of *Il6* and *Ucp1* relative expression in mouse adipocytes, each data point represents a biologically independent sample. **(D)** SDH-A levels in adipocytes transfected with mtRNA. Anti-IL-6: cells were incubated with an antibody against IL-6. STAT-3 blockage: cells were treated with the JAK2/STAT3 inhibitor ruxolitinib. N = 3 biologically independent samples. **(E)** Transcription of beige adipocyte genes in mouse adipocytes treated with vehicle, 10 ng/ml IL-4, 200 pg/ml IL-6 or 2 μg/ml mtRNA for 18 h. N = 3 N = 6 biologically independent samples. **(F)** Expression of beige adipocyte genes in adipocytes treated with the JAK2/STAT3 inhibitor ruxolitinib as described[16]. N = 3 biologically independent samples. Data are represented as mean ± SEM. Statistical significance was determined using Student's 2-tailed unpaired *t*-test.
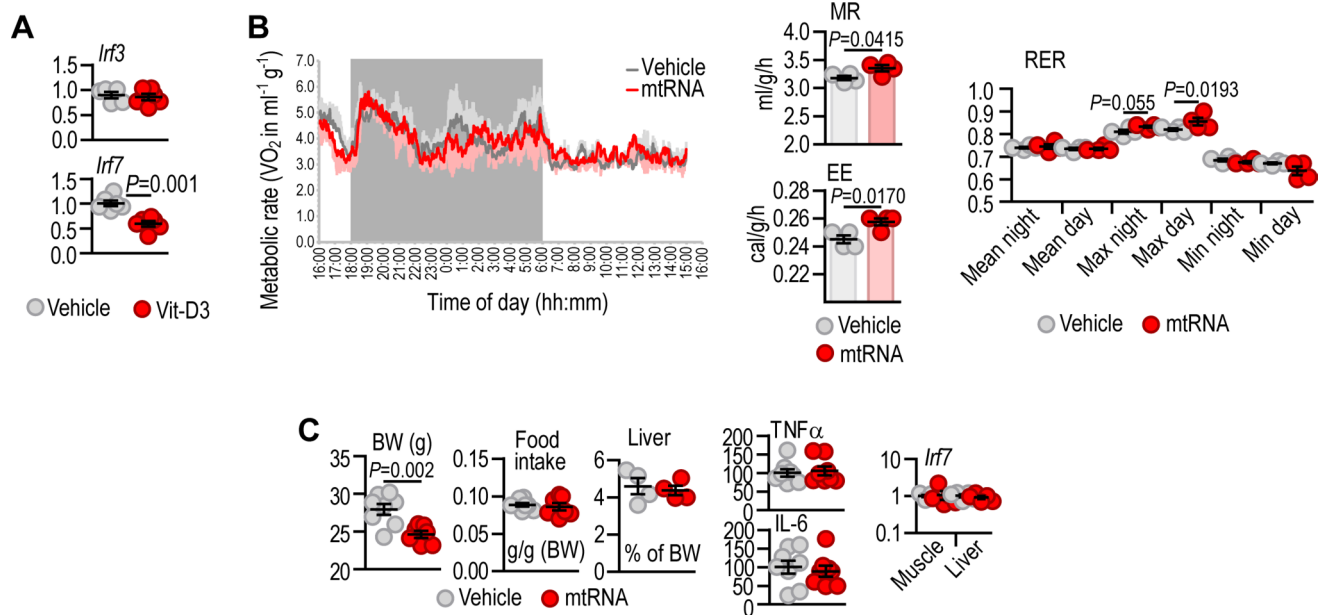
Extended Data Fig. 7 | Metabolic role of mtRNA-mediated signaling. (A) Level of *Irf3* and *Irf7* in mouse adipocytes treated with 1 μM Vit-D3 for 18 h. N = 6 biologically independent sample. (**B**) Indirect calorimetry assay of high-fat diet (HFD)-fed adult male C57BL/6 mice, N = 6 biologically independent samples. The inguinal fat depot was transfected with vehicle or with 0.6 μg/g body weight (BW) per day mtRNA for 14 days. The mtRNA was delivered into the adipocyte cytoplasm using magnetofection. Both groups received 4 ng/g BW Vit-D3 daily.

MR: metabolic rate, EE: energy expenditure, RER: respiratory exchange rate (**C**) BW, daily food intake normalized to BW (N = 8 biologically independent samples), and liver weight normalized to BW (N = 4 biologically independent samples). Plasma level of TNFα and IL-6 (% of vehicle) from vehicle- or mtRNA-transfected mice, and the level of *Irf7* in quadriceps muscle and liver (N = 8 biologically independent samples). Data are represented as mean ± SEM. Statistical significance was determined using Student's 2-tailed unpaired *t*-test.
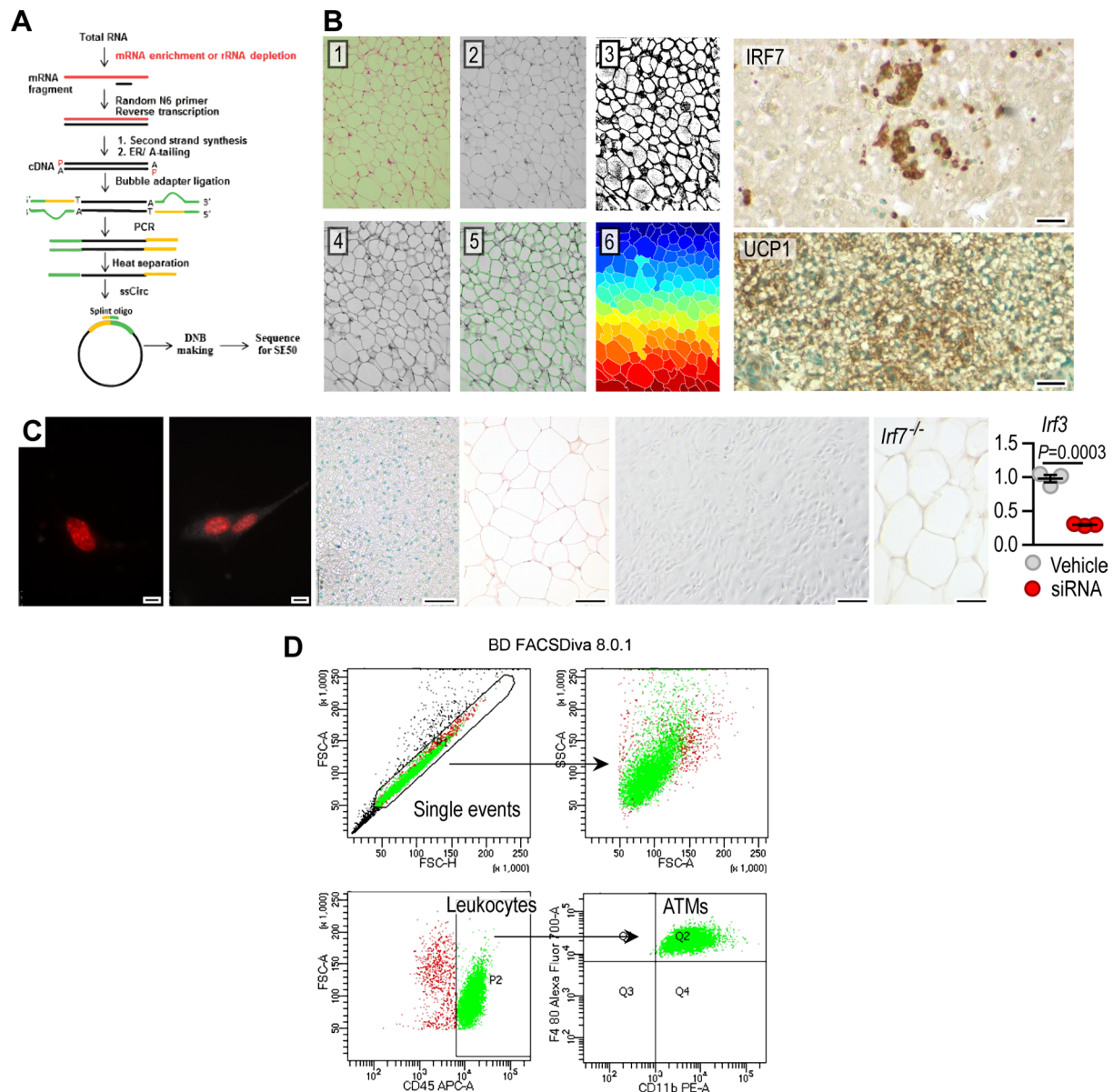
Extended Data Fig. 8 | Technical information on next-generation sequencing and image analysis. (**A**) Workflow of the next-generation sequencing analysis. (**B**) Left: Steps of image analysis in histomorphometry [1-6]. Right: Positive controls in immunohistochemistry. Newborn liver was used for testing IRF7 antibody. Note the hematopoietic cell foci. Brown adipose tissue of mouse was used as a control for UCP1 antibody. Methyl-green counterstaining for nuclei. Further validation provided in ref. [11]. Scale 50 μm. Performed three times.

(**C**) Negative control specimens. *Left:* Adipocytes *in vitro*, stained with secondary antibodies only; nuclei are labeled with DAPI. Scale: 10 μm. *Middle:* Mouse brown adipose tissue section labeled with secondary antibody only. Human adipose tissue labeled with secondary antibody only. Scale: 20 μm. *Right:* Adipose tissue of an IRF7-deficient mouse labeled with an antibody against IRF7. *Irf3* level in 3T3-L1 cells transfected with *Irf3* siRNA for 48 h. (**D**) Example of adipose tissue macrophage (ATM) gating strategy. Further details in refs. [97] and [113].

nature portfolio

Corresponding author(s): Tamás Röszer

Last updated by author(s): Sep 27, 2022

Reporting Summary

Nature Portfolio wishes to improve the reproducibility of the work that we publish. This form provides structure for consistency and transparency in reporting. For further information on Nature Portfolio policies, see our Editorial Policies and the Editorial Policy Checklist.

Statistics

For all statistical analyses, confirm that the following items are present in the figure legend, table legend, main text, or Methods section.

n/a	Confirmed	
☐	☒	The exact sample size (*n*) for each experimental group/condition, given as a discrete number and unit of measurement
☐	☒	A statement on whether measurements were taken from distinct samples or whether the same sample was measured repeatedly
☐	☒	The statistical test(s) used AND whether they are one- or two-sided *Only common tests should be described solely by name; describe more complex techniques in the Methods section.*
☒	☐	A description of all covariates tested
☐	☒	A description of any assumptions or corrections, such as tests of normality and adjustment for multiple comparisons
☐	☒	A full description of the statistical parameters including central tendency (e.g. means) or other basic estimates (e.g. regression coefficient) AND variation (e.g. standard deviation) or associated estimates of uncertainty (e.g. confidence intervals)
☐	☒	For null hypothesis testing, the test statistic (e.g. F, t, r) with confidence intervals, effect sizes, degrees of freedom and P value noted *Give P values as exact values whenever suitable.*
☒	☐	For Bayesian analysis, information on the choice of priors and Markov chain Monte Carlo settings
☒	☐	For hierarchical and complex designs, identification of the appropriate level for tests and full reporting of outcomes
☒	☐	Estimates of effect sizes (e.g. Cohen's *d*, Pearson's *r*), indicating how they were calculated

Our web collection on statistics for biologists contains articles on many of the points above.

Software and code

Policy information about availability of computer code

Data collection	QuantStudio™ Design & Analysis Software, Thermofisher Scientific v1.5.0 (for qPCR); Leica Application Suite X Leica 3.7.2.22383 (for microscopy of immunofluorescence); Olympus CellSense Entry Olympus 2.3 (for histology imaging and cell culture imaging); Leica Application Suite Z Leica 3.4.0 (for histology imaging); Motic Images Plus 3.0 V137 (for histology imaging); AUTOsoft Autobio Co. LTD 2.6.9 (for ELISA); Fusion FX6 Edge Vilber 18.02 and NanoDrop 2000/2000c Thermofisher Scentific 1.6.198 (for RNA quantity)
Data analysis	Workflow described in the Supplementary Information. We used Excel, GraphPad Prism, FlowJo, ImageJ for data analysis.

For manuscripts utilizing custom algorithms or software that are central to the research but not yet described in published literature, software must be made available to editors and reviewers. We strongly encourage code deposition in a community repository (e.g. GitHub). See the Nature Portfolio guidelines for submitting code & software for further information.

Data

Policy information about availability of data

All manuscripts must include a data availability statement. This statement should provide the following information, where applicable:
- Accession codes, unique identifiers, or web links for publicly available datasets
- A description of any restrictions on data availability
- For clinical datasets or third party data, please ensure that the statement adheres to our policy

Data are available for secondary use upon request, and key experimental data are accessible via Figshare. Flow Repository identifiers of FACS data are as follows: #FR-FCM-Z236, #FR-FCM-Z2R6, #FR-FCM-ZYPU, #FR-FCM-ZYUU, FR-FCM-Z5QA. NGS data are deposited at GEO with the accession number #GSE185317. For secondary analysis, we used our previously published NGS datasets, with accession numbers #GSE125405 and #GSE133500.

Field-specific reporting

Please select the one below that is the best fit for your research. If you are not sure, read the appropriate sections before making your selection.

[✗] Life sciences   [ ] Behavioural & social sciences   [ ] Ecological, evolutionary & environmental sciences

For a reference copy of the document with all sections, see nature.com/documents/nr-reporting-summary-flat.pdf

Life sciences study design

All studies must disclose on these points even when the disclosure is negative.

Sample size	The overall experimental design has been apprpved and sample size has been deterimined by a prior analysis conducted by a biostatistician. In brief, sample size calculation was based on the expected, biologically relevant difference in the measured parameter between the control and the test group (e.g., vehicle vs. treated; young vs. adult, etc.). Assuming normally distributed data from these quasi-continuous endpoints with a power of 80% and a two-sided type 1 error of 5%, the t-test for parallel groups was used to estimate the number of cases. Due to its multi-factorial setting, the experiments are evaluated with methods of analysis of variance (ANOVA) in the case of steady, normally distributed target variables. Corresponding non-parametric methods (e.g., Kruskal-Wallis) were used for data that are not normally distributed. The t-test or the Wilcoxon test for unrelated samples was used for two-group comparisons. Qualitative parameters are evaluated with the chi-square test or the exact test according to Fisher. Before the start of the statistical test evaluation, all parameters were descriptively analyzed according to their characteristics.
Data exclusions	Prior analysis exlclusion: experimental animals were excluded from the study based on a priori described featrues (e.g., apparent sickness, excessive weight loss, in-cage aggression, etc.). In case of human subjects, a priori exclusion criteria included chronic inflammatory disease, actue infection, surgical complication (e.g., excessive bleeding). Following data collection data were excluded only if a justified technical issue during data collection was proven.
Replication	Key exepriments have been replicated by two independent researchers with similar outcome. Assays presented in the manuscript have been replicated successfully at least two independent times.
Randomization	Animals were randomized to assign them to control and test groups in the case of intervention studies (i.e., treating animals with vehicle or test compounds or high fat diet), by randomly selecting their numerical identification numbers. These identification numbers were generated using their cage identification numbers and date of birth. In case of human subjects we did not conduct intervention studies, and human fat samples were analysed on the day of surgery of the donor patients. Order of surgery was determined by the surgical team, and all patients at our surgery departments - apart from those who met some exlcuison criteria - were approached by the surgeon with the possibility of participating in the study, giving no reason for further randomizing samples.
Blinding	All samples were labeled with numerical codes, allowing blinding in data analysis, and investigators were blinded to gorup allocation during data collection.

Reporting for specific materials, systems and methods

We require information from authors about some types of materials, experimental systems and methods used in many studies. Here, indicate whether each material, system or method listed is relevant to your study. If you are not sure if a list item applies to your research, read the appropriate section before selecting a response.

Materials & experimental systems

n/a	Involved in the study
[ ]	[✗] Antibodies
[ ]	[✗] Eukaryotic cell lines
[✗]	[ ] Palaeontology and archaeology
[ ]	[✗] Animals and other organisms
[ ]	[✗] Human research participants
[ ]	[✗] Clinical data
[✗]	[ ] Dual use research of concern

Methods

n/a	Involved in the study
[✗]	[ ] ChIP-seq
[ ]	[✗] Flow cytometry
[✗]	[ ] MRI-based neuroimaging

Antibodies

Antibodies used	The complete antibody list is provided in Supplementary Table 2, along with their source, clone number and dilution.
Validation	Manufacturers of the used antibodies (listed in Supplementary Table 2) provided validation data of each antibody. We further performed postve and negative staining assays as shown in Extended Data Figure 8. In brief, as IRF7 positive control we used hematopoietic foci of newborn liver specimens, for UCP1 mouse interscapular adipose tissue specimens. As negative control we omitted primary antibodies in the staining procedure. We also used adipose tissue from IRF7 deficient adult mice for IRF7 immunostaining as negative control. Further validation of UCP1 labeling is provided in Cells

Eukaryotic cell lines

Policy information about cell lines

Cell line source(s)	3T3-L1 and THP-1 cell lines were obtained from ATCC.
Authentication	Expression of characteristic mRNA transcripts (e.g., Ifi204, Ifi203, Ifi202b of BALB/C origin, Fabp4 and Fasn for lineage identity; morphology (with phase contrast and with transmission electron microscopy) and cell-line specific behavior (i.e., adipogenic differentiation) have been tested for 3T3-L1 cells. For THP-1 cells morphology (monocytic or induced adheren macrophage-like), activation in response to stimuli were used to ensure lineage identity.
Mycoplasma contamination	The cell lines were regularly tested negative for Mycoplasma.
Commonly misidentified lines (See ICLAC register)	Not applicable (our cell lines are not listed in ICLAC register, as of October 26, 2021).

Animals and other organisms

Policy information about studies involving animals; ARRIVE guidelines recommended for reporting animal research

Laboratory animals	mouse, Mus musculus, C57BL/6 as wild-type, MDA5-KO and IRF7-KO on a C57BL/6 background, RIG-I-KO on CD1 background (for this we used CD1 as control). Housing conditions: 12h/12h day/might cycle, under SPF health monitoring, in individually ventilated cages, at ambient temperature (20-22°C) and at 55% air humidity. Animals were housed 1 animal per cage (during high-fat diet and indirect calorimetry) or in groups with bedding and paper nesting material. The animals could move freely. The cages stood next to each other so that the animals have visual contact. The animals were given ad libitum access to water and food. As standard protocol at Ulm University, the requirements of ETS123 were met.
Wild animals	none
Field-collected samples	none
Ethics oversight	Research involving animals was approved by the regional governmental ethics and animal welfare committee in Tübingen, Germany (#1511; #1557; #1492; #1546; #o.232-1,2,4,5). Study approvals are available upon request in German.

Note that full information on the approval of the study protocol must also be provided in the manuscript.

Human research participants

Policy information about studies involving human research participants

Population characteristics	Study Population: children and adolescents undergoing elective surgery at the University Hospital Leipzig, Germany and Pediatric Surgery Department, Institute of Pediatrics, University of Debrecen, Hungary, between 2010 and 2022. Indication of surgery: retentio testis, hydrocele, hernia, collar fistula, naevus removal, stoma closure, gynecomastia,anal fistula, other The study cohort may be stratified for lean (definded as BMI <1.28 SDS) and overweight/obese (definded as BMI>= 1.28 SDS) children for posthoc analyses, no intervention. Inclusion Criteria: 1. body weight: 3000 g - 180 kg 2. suitable surgical procedure 3. signed informed consent by the guardians and the study participant, if older 12 years (Germany), or signed informed consent by the guirdans of the study participants under 18 years of age (Hungary) Exclusion Criteria: 1. severe chronic and inflammatory diseases 2. acute or chronic infections 3. oncological diseases 4. clotting disorders 5. complications during surgical procedure 6. drug treatment Age range of participants: 0-18 years Sex of participants: male (65%), female (35%). The higher percentage of male participants was due to the higher rate of medical conditions among males in pediatric surgery practice (i.e., surgical resolution of retentio testis or testicular torsion apply only to boys, and inguinal hernia is more common among boys than girls).
Recruitment	Participants underwent elective surgery at University Hospital of University of Leipzig, Germany between 2010 and 2020 or at Pediatric Surgery Department, Institute of Pediatrics, University of Debrecen, Hungary in 2022 (children and adolescents). Recruitment from 2010 to 2022. Data collection for Illumina and histology/FACS/immunofluorescence analysis: 2010-2021,

functional assays/FACS: 2022. Parents or guardians of the patients were contacted by the surgeon before the surgery, providing informed consent abut the study. There is self-selection bias involved, as participants did not actively apply for participation in the study. Since each patient in the indicated time period of recruitment was approcahed with the information on our study (unless an exclusion criteria was apparent for the surgeon), there is no recruitment bias. Parents/guardians were free to accept or decline the participation in the study, and they receibed sufficient time to make a decision. The study cohort may be stratified for lean (definded as BMI <1.28 SDS) and overweight/obese (definded as BMI>= 1.28 SDS) for posthoc analyses, no intervention. Patient selection was not affected by the BMI SDS, gender or other clinical parameter, to avoid recruitment bias.

Ethics oversight	The study protocol was approved by the local ethics committee of the Medical Faculty, University of Leipzig (#265-08-ff; NCT02208141) and the Medical Faculty of University of Debrece (#RKEB6057).

Note that full information on the approval of the study protocol must also be provided in the manuscript.

Clinical data

Policy information about clinical studies

All manuscripts should comply with the ICMJEguidelines for publication of clinical research and a completedCONSORT checklist must be included with all submissions.

Clinical trial registration	NCT02208141

Study protocol	https://clinicaltrials.gov/ct2/show/NCT02208141

Data collection	Participants of this study were undergoing elective surgery at the University Hospital Leipzig, Germany and Pediatric Surgery Department, Institute of Pediatrics, University of Debrecen, Hungary, between 2010 and 2022. Recruitment period was between 2010-2022. Parents/guirdans of each eligible patient was approached by one member of the surgical team, to prvide information about our study, answer questions of the parents/guirdans, and ensure that all necessary documents (informed consent, data protection, etc.) are signed and archived. There is no self-selection bias in the study participation.

Outcomes	Primary Outcome Measures : Adipose tissue dysfunction [Time Frame: 10 years] Adipose tissue dysfunction is assessed by evaluation of adipocyte size and number (hypertrophy vs. hyperplasia), adipocyte proliferation and differentiation, (lipid) cellular metabolism, inflammation, gene expression, fibrosis, and others; the association of AT dysfunction with clincial phenotype will be assessed Secondary Outcome Measures : Presence of beige/brown adipose tissue (BeAT/BAT) [Time Frame: 10 years] Adipose tissue samples are evaluated for the presence of BeAT/BAT on histological and molecular level and association with clinical phenotype isinvestigated Inflammation of adipose tissue [Time Frame: 10 years] Inflammation is assessed by evaluating macrophage infiltration on histological and molecular expression level. Also, association with clinical phenotype is assessed. Biospecimen Retention (Leipzig only): samples with DNA adipose tissue sample mRNA from adipose tissue samples, adipocytes, stromal vascular fraction protein from whole adipose tissue samples blood samples for DNA analysis, serum samples urine samples Biospecimen Retention (Debrecen only): adipose tissue sample patient charts (follow-up of clinical phenotype)

Flow Cytometry

Plots

Confirm that:

[x] The axis labels state the marker and fluorochrome used (e.g. CD4-FITC).

[x] The axis scales are clearly visible. Include numbers along axes only for bottom left plot of group (a 'group' is an analysis of identical markers).

[x] All plots are contour plots with outliers or pseudocolor plots.

[x] A numerical value for number of cells or percentage (with statistics) is provided.

Methodology

Sample preparation	Fat samples were digested with collagenase, followed by separation of cell fractions and subsequently analyzed or cultured, as described: Ampem G, and Röszer T. In: Badr MZ ed. Nuclear Receptors: Methods and Experimental Protocols. New York, NY: Springer New York; 2019:225-36. ATMs were purified before FACS analysis with magnetic bead labeling and sorting, as described in the Supplementary Information.
Instrument	BD LSR II
Software	FlowJo v10, FACSDiva 8.01
Cell population abundance	2,000-10,000 cells.
Gating strategy	Single cell events are gated first, adipocyte and ATM populations second (based on SSC-A and FSC-A parameters), this is fllowed by gating for primary antibody signals (e.g., F4/80). Details provided in reference: Ampem G, and Röszer T. In: Badr MZ ed. Nuclear Receptors: Methods and Experimental Protocols. New York, NY: Springer New York; 2019:225-36., also shown in SFig. 15D

☒ Tick this box to confirm that a figure exemplifying the gating strategy is provided in the Supplementary Information.